5 Parameter Identification by Numerical Program

5.1 Objectives of Application of the Numerical Method

The objectives of the numerical parameter identification, which has been developed in the present studies, is to evaluate all the parameters stepwise with repeated reference of various experimental data. The numerical method is carried out on the computer to allow a number of repetitions between each reference of experimental behavior and treats great amount of numerical data obtained from cyclic tests and succeeding relaxation tests for the elaborated exactitude based on a least square curve fitting method. The most important advantage of employing a numerical determination method is that an evaluated parameter set can be confirmed its physical properties through repeated comparison with the experimental behaviors.

In this chapter, the numerical procedure is applied to evaluate the parameter sets for two different temperature cases of T = 200℃ and 400℃ independently based on the experimental data on a computer. The seven parameters included in Chaboche's model are dependent on temperature and should be determined under the both temperature conditions. The numerical program for the simulation of the stress-strain histories with a parameter set, which was employed in Chapter 3, is used to compare the simulation behavior by the evaluated parameter set with the experimental behavior and to modify the parameter values slightly.

5.2 Identification Procedures

5.2.1 Overview of the Parameter Evaluation Procedures

Essentially, the curve fitting in this identification method is carried out base on a least square method, i.e., the sets of stress σ and inelastic strain rate $\dot{\varepsilon}^p$ obtained from experiments are led into the Chaboche's constitutive equations, and the accurate parameter set, which shows the most similar relationship between the stress and the inelastic strain rate, is evaluated. Needless to

mention, the more accurate parameter set can be expected from the more number of data.

The flow chart of the parameter evaluation procedure, which was developed in the present studies, is shown in Figure 5.2.1.1. The procedure can mainly be divided into three steps of parameter evaluation and two steps of their confirmation. Through evaluation procedure 1, the experimental data of cyclic tests should be arranged to evaluate parameters K, n, H and D. Through evaluation procedure 2, parameters K and n are evaluated based on the experimental data of relaxation test. The evaluated parameter sets K and n are checked their values through confirmation procedure 1. If necessary, they should be adjusted with these cyclic and relaxation data to be re-evaluated from the beginning of evaluation procedure 1. After some iterations, these parameter values predicted with the experimental data of cyclic hysteresis curves and relaxation curves are obtained. Then, through evaluation procedure 3, parameters h, d and k can be evaluated based on the stress history at the hysteresis tips. Through confirmation procedures 2, all the parameters are confirmed with cyclic, relaxation and cyclic hardening simulations with the evaluated parameter set. Since the predicted values of Chaboche's parameters are to be used to the fatigue behavior calculation, Procedure 1 is considered to be essential, while other procedures are also necessary to give the physical significance to the parameter set. Each procedure will be explained in the following sections.

Through these procedures, the parameters included in the uniaxial form of Chaboche's constitutive equations can be determined stepwise and iteratively based on the results of cyclic tests and succeeding relaxation tests. Three parameter groups of (K and n), (K, n, H and D) and (h, d and k) can be evaluated independently base on the relaxation behavior, the cyclic hysteresis behavior and the cyclic strain hardening behavior obtained from experiments in the procedures. Then, these parameter groups are to be compared and modified to the more accurate values with reference to various experimental behaviors through a number of repeated evaluations over the parameter values of each group.

As to the cyclic behavior, a number of hysteresis curves nearly after the saturation, for examples, the twenty-forth, the thirtieth, the forty-eighth and the sixtieth cycles of each hysteresis curve and some other cycles with different strain rate, strain range or mean strain value were referred. As to the relaxation behavior, all the experimental curves were referred with different holding strains. For the hardening behavior, all the histories of the stress value at the hysteresis tip with different loading conditions were referred. Reference to different loading conditions reduces error of the parameter evaluation and material scattering.

5.2.2 Treatment of the Experimental Data

One of the advantages of the procedures is that several experimental data obtained from different test specimens can be taken into consideration to evaluate the parameter set. The experimental data were numerically recorded onto floppy disks and directly fed into the computational program. While the cyclic hysteresis curves can be obtained without large experimental error (for examples, milled curvatures on the experimental curves), the relaxation curves can not get rid of such error

since the relaxation behavior of type SS 316L SPH stainless steel is not so considerably accurate (i.e., it has no large viscoplastic characteristics). Using the relaxation data directly without any treatment, the numerical procedure can hardly calculate the accurate parameter values of K and n.

Therefore, smoothing and digitalization of the relaxation data are necessary before the numerical parameter identification. However, it is difficult to smooth the numerically recorded relaxation data of stress histories directly. Thus, in the present studies, the graphically recorded data were used to be smoothed and then the smoothed curves were digitalized to be transferred as the stress histories of relaxation tests onto floppy disks. The smoothing work was carried out by hands, and the digitalization was done by means of a plotting tool. (The whole procedures to use the original relaxation data will be shown in Figure 5.2.3.1 later.)

5.2.3 Details of the Procedures

Evaluation procedure 1 :

The parameters K, n, H and D were evaluated from the hysteresis loops of the saturated cycles, where R is a constant. (In fact, it need not be that the reference cyclic loops are after the saturation, while R can be treated as the R value of each referred cycle before the saturation. The evaluation results, however, become better if no unsaturated cyclic loop is referred to evaluate the parameters, which will be discussed in Chapter 8.) The stress is given by the sum of back stress, yield stress R and over stress Z as follows :

$$\sigma = \frac{H}{D}(1 - c\, e^{-PD}) + R + K\sqrt[n]{\dot{\varepsilon}^p} \qquad (5.2.3.1)$$

where

$$P = \int d\left|\dot{\varepsilon}^p\right| \qquad (5.2.3.2)$$

The constant c can be determined unambiguously on the basis of the initial condition of back stress for symmetric hysteresis loops. P is the accumulated plastic strain rate. By means of a least square method, relationship 5.2.3.1 is fitted to the experimental hysteresis curves.

Evaluation procedure 2 :

The cyclic loop is actually almost independent of the strain rate, i.e., over stress is too small to determine reliably parameters K and n. On the other hand, variation in over stress is significant throughout the relaxation tests. Therefore, in this procedure, the evaluated parameters K and n should be confirmed by the experimental data of the relaxation tests. From the relaxation data of stress-time histories, stress-inelastic strain rate relations can be obtained based on the relaxation condition of the stationary strain as shown in Figure 5.2.3.1 (which has already been explained with equation 4.3.3.1). Here, yield stress R has already been saturated since all tests were performed after pre-cycles (stress value is equivalent to the sum of yield stress R and back stress Y at the saturation of relaxation curve), and the back stress Y can be calculated with the obtained

parameters H and D analogously to evaluation procedure 1. Then, only the parameters K and n are to be determined by fitting the simulated stress behavior to the experimental one, which is based on a least square method.

Confirmation procedure 1 :

After these evaluations, the parameter sets of K and n obtained from evaluation procedures 1 and 2 should be compared with each other. If the disagreement between these two parameter sets is appreciable, these two evaluation steps must be repeated from the beginning with slight modification of parameter values K, n, H and D in evaluation procedure 1 to the average of previous two different evaluation results. Here, the slight modification of the parameters needs skill on the characteristics of Chaboche's parameters influence to various material behaviors as simulated in Chapter 3.

Evaluation procedure 3 :

The remaining parameters d, h and $k = R_0$ are to be evaluated from the hysteresis tips of the stress histories of cyclic tests. Since parameters K, n, H and D are known, correlation 5.2.3.1 involves only an unknown term of R. At the hysteresis tip, values of the first term and the third term can be calculated and the following relationship holds :

$$\sigma_{tip} = Y_{tip} + [\, k + \frac{h}{d}(1 - e^{-P_d}) \,] + Z_{tip} \qquad (5.2.3.3)$$

where Y_{tip} and Z_{tip} are known as functions of K, n, H and D as follows :

$$Y_{tip} = \frac{H}{D}[\, 1 - c \times \exp(- P_{tip} D) \,] \qquad (5.2.3.4)$$

$$Z_{tip} = K\sqrt[n]{\dot{\varepsilon}^{P}_{tip}} \qquad (5.2.3.5)$$

Again, parameters R_0, h and d are determined by means of a least square method.

Confirmation procedure 2 :

Finally, cyclic, simple tensile and cyclic hardening behaviors should be simulated by the constitutive equations with the obtained parameter set to be compared with the experimental curves. If the disagreement between these behaviors is found appreciable, the procedure must be repeated from the beginning with slight modification of parameter values K, n, H and D in evaluation step 1 so as to give the better simulation with experimental data. Here, slight modification also needs skill on the characteristics of Chaboche's parameters influence to the various material behaviors. In this study, fitting to the cyclic behavior is especially important because the first wall condition of the thermo-mechanical cyclic loading is taken into consideration. This final confirmation is the most important and the most typical procedure through the newly developed numerical parameter identification method to refer several experimental behaviors to the parameter set.

5.3 Results of Parameter Evaluation

5.3.1 Values of the Evaluated Parameters

After several iterations among these three steps mentioned above, some parameter sets were obtained for temperature conditions of T = 200℃ and 400℃. With these parameter sets, cyclic curves and cyclic hardening curves were simulated and were compared with the corresponding experimental data to choose the best parameter set.

The final parameter sets are shown in Table 5.3.1.1 for each temperature value. These final parameter sets were determined because their stress values at the hysteresis tip of the saturated cycle, their curvatures of the saturated hysteresis loop and their curvatures of cyclic hardening behavior were the best fitted to the experimental data. (The error introduced in the parameter evaluation will be discussed in Chapter 8.)

5.3.2 Comparison between Fitted and Experimental Curves

Cyclic loading simulations, relaxation simulations and cyclic hardening simulations by Chaboche's model with these parameter sets are shown in this section with the corresponding experimental data for each temperature value, respectively. These behaviors were directly referred to fit the parameters to them.

For cyclic behaviors, Figures 5.3.2.1 and 5.3.2.2 show the cyclic hysteresis curves for temperature cases of T = 200℃ and 400℃ with strain range of $\Delta\varepsilon = 0.4\%$, which were simulated by Chaboche's model with the evaluated parameter sets. Figures 5.3.2.3 and 5.3.2.4 correspond to those with strain range of $\Delta\varepsilon = 0.6\%$. Slight disagreement of 4% (in the case of strain rate $\dot{\varepsilon} = 2.0 \times 10^{-4}$ /sec and strain range $\Delta\varepsilon = 0.4\%$ under temperature condition T = 200℃) to 11% (in the case of strain rate $\dot{\varepsilon} = 2.0 \times 10^{-4}$ /sec and strain range $\Delta\varepsilon = 0.6\%$ under temperature condition T = 200℃) at the hysteresis tips (both at the maximum and the minimum stress points) is smaller than that of over 15% in the previous studies. The confirmation of the hysteresis loops gives good agreement on the curvature between the experimental and the simulated curves.

As to relaxation behaviors, Figures 5.3.2.5 and 5.3.2.6 show the over stress lines, which were simulated by Chaboche's model with the evaluated parameters K and n, within the experimental data scattering. That means the simulated over stress lines agree well with the experimental data within the scope of experimental errors. The relaxation behaviors simulated by the evaluated parameter sets for two temperature cases are shown in Figures 5.3.2.7 and 5.3.2.8. The relaxation data are sufficiently fitted.

As to cyclic hardening behaviors, Figures 5.3.2.9 and 5.3.2.10 show the cyclic hardening curves, which were simulated by the Chaboche's model with the evaluated parameter sets, also within the experimental data scattering. The good agreement on this behavior is also very important, which suggests the evaluated parameters can satisfy their validity to the fatigue conditions with shifted strain conditions (especially different strain ranges). Agreement between the simulated results and the experimental data was also satisfactory.

5.3.3 Other Material Behaviors with the Evaluated Parameters

Tensile and cyclic strain hardening behaviors simulated by the evaluated parameter sets are shown here. Figures 5.3.3.1 and 5.3.3.2 show the tensile curves calculated by Chaboche's model for two temperature cases of T = 200℃ and 400℃, respectively. Figures 5.3.3.3 and 5.3.3.4 show the cyclic strain hardening curves calculated by Chaboche's model for two temperature cases of T = 200℃ and 400℃, respectively.

These behaviors were fitted not completely but tolerably because these behaviors can be regarded not so important as the cyclic behavior or the cyclic hardening behavior in the present studies. Comparison of these simulated curves with experimentally obtained ones will be discussed in Chapter 8, while the agreement between the simulated and the experimental curves is sufficient for each temperature case.

Table 5.3.1.1 : Evaluated results for two temperature cases

Temperature	K	n	H	D
200℃	0.87×10^{2}	4.93	1.69×10^{5}	1.65×10^{3}
400℃	1.03×10^{2}	3.27	1.08×10^{5}	1.13×10^{3}

Temperature	h	d	k
200℃	1.32×10^{2}	1.13	1.02×10^{2}
400℃	5.83×10^{2}	4.89	0.63×10^{2}

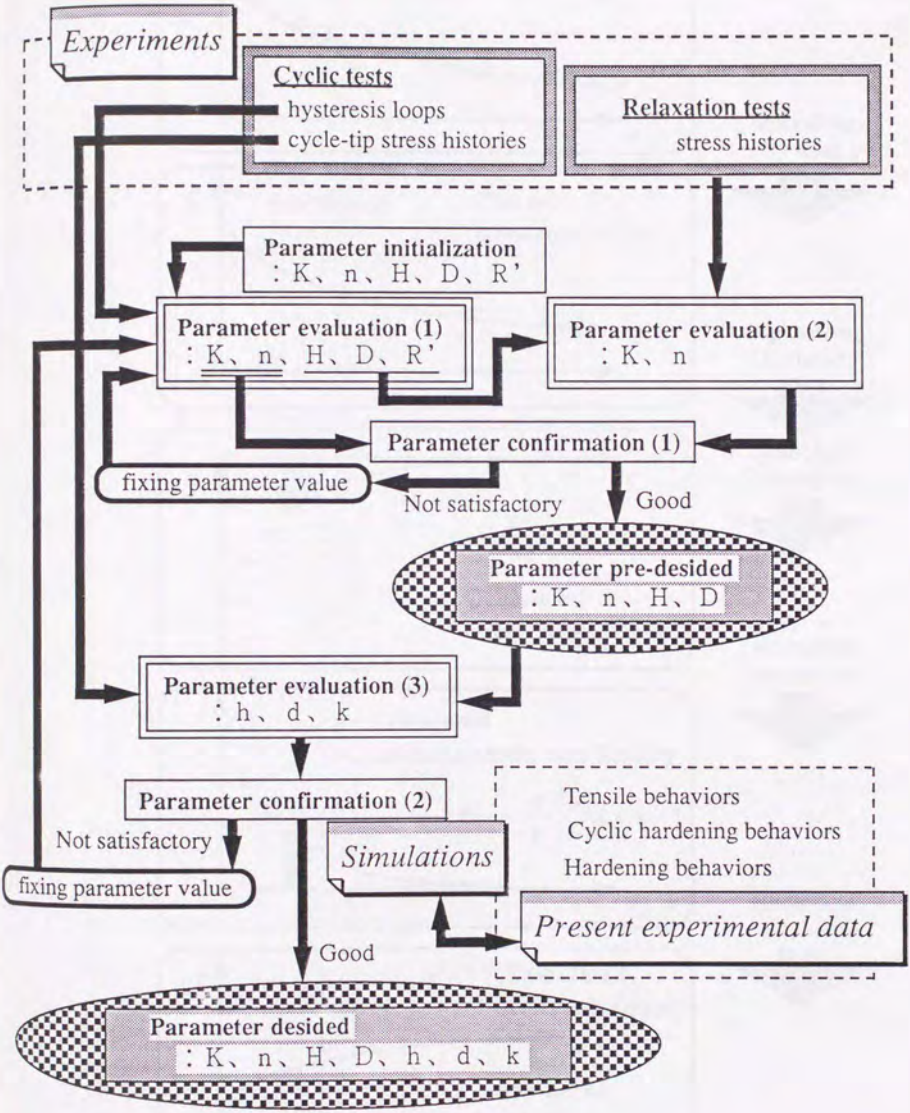

Figure 5.2.1.1 : Flow chart of the numerical identification method

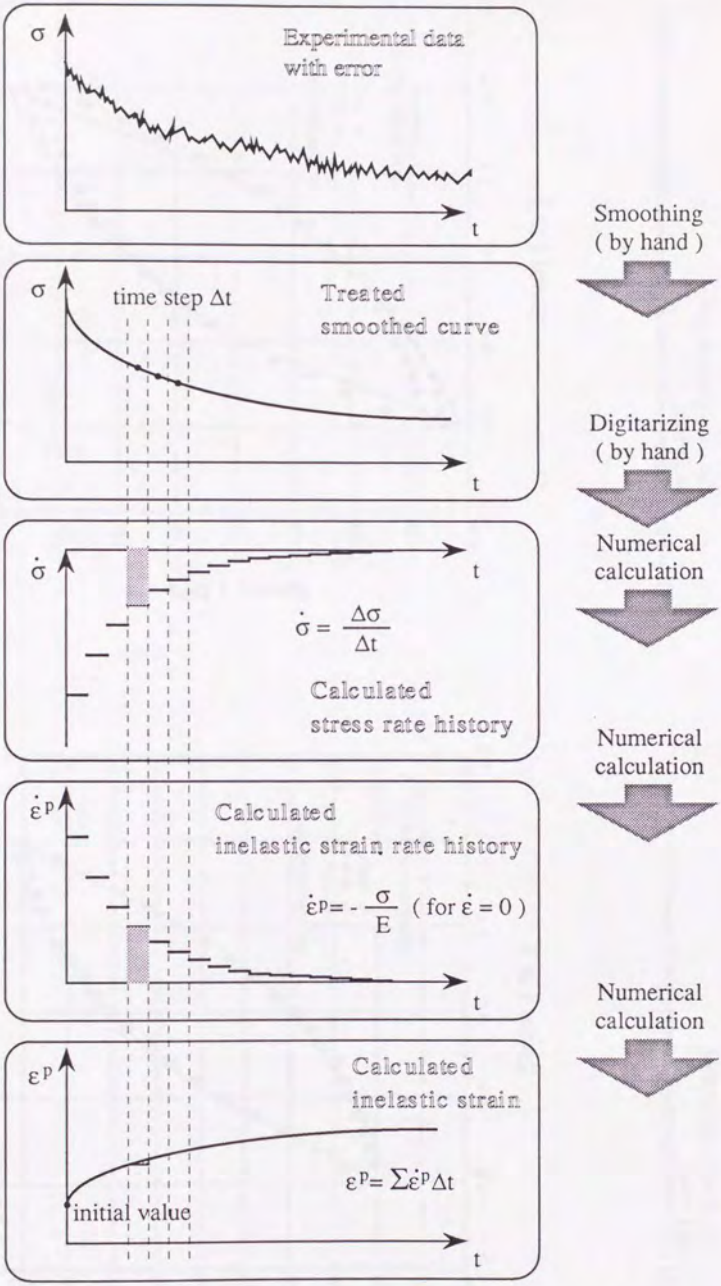

Figure 5.2.3.1 : Data treatment for relaxation results

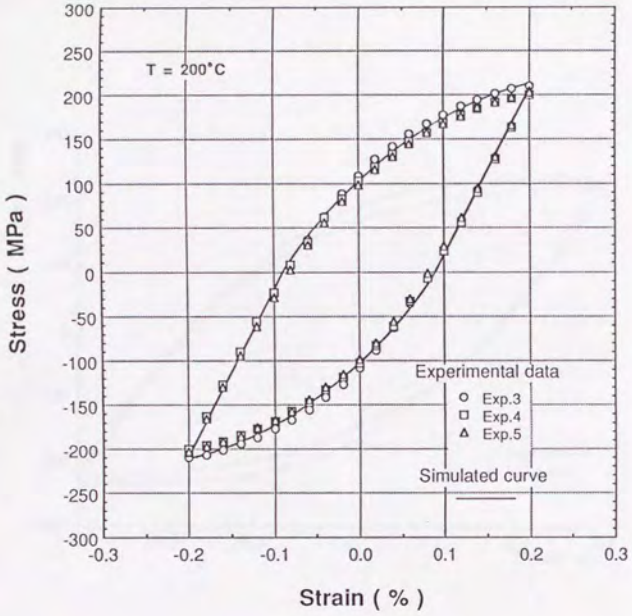

Figure 5.3.2.1 : Cyclic behavior by Chaboche's model compared with experimental curve for T = 200℃
($\Delta\varepsilon = 0.4\ \%$, $\dot{\varepsilon} = 2.0 \times 10^{-4}$/sec)

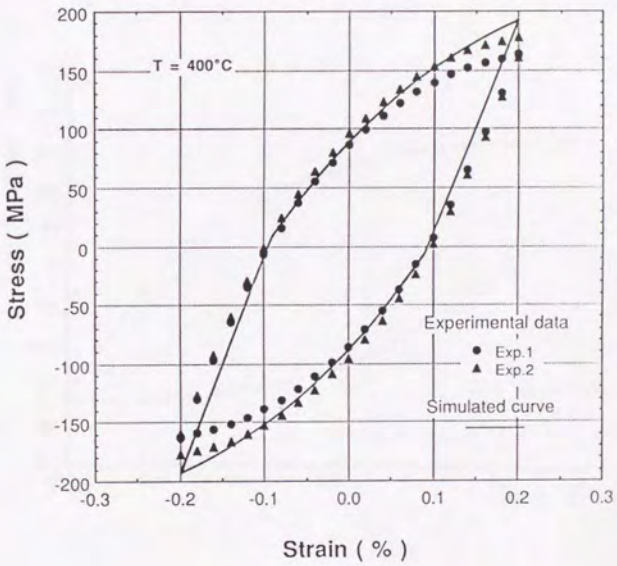

Figure 5.3.2.2 : Cyclic behavior by Chaboche's model compared with experimental curve for T = 400℃
($\Delta\varepsilon = 0.4\ \%$, $\dot{\varepsilon} = 2.0 \times 10^{-4}$/sec)

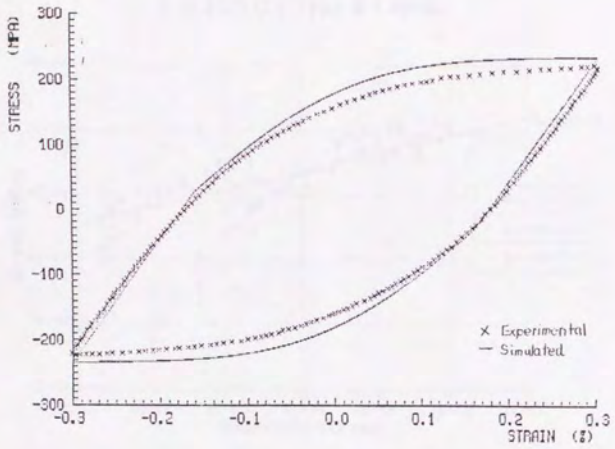

Figure 5.3.2.3 : Cyclic behavior by Chaboche's model compared with experimental curve for T = 200℃
($\Delta\varepsilon = 0.6\ \%$, $\dot{\varepsilon} = 2.0 \times 10^{-4}$/sec)

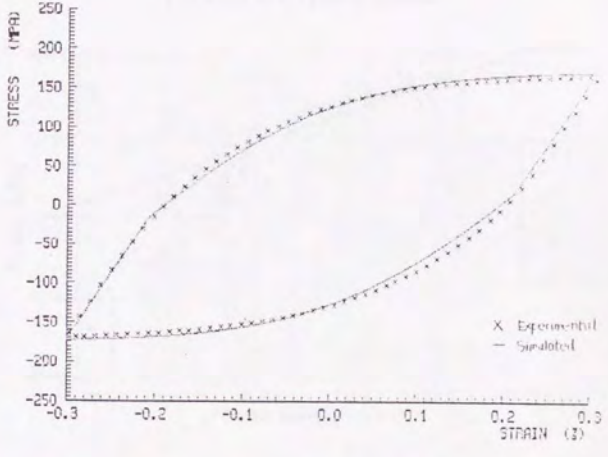

Figure 5.3.2.4 : Cyclic behavior by Chaboche's model compared with experimental curve for T = 400℃
($\Delta\varepsilon = 0.6\ \%$, $\dot{\varepsilon} = 2.0 \times 10^{-4}$/sec)

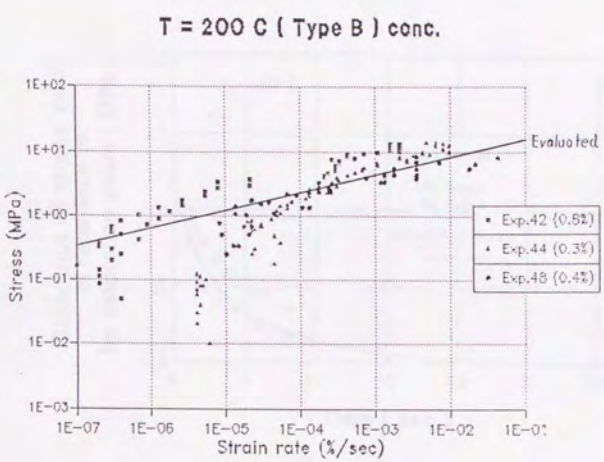

Figure 5.3.2.5 : Over stress behavior by Chaboche's model compared with experimental data
T = 200℃ (hold strain value = 0.4%)

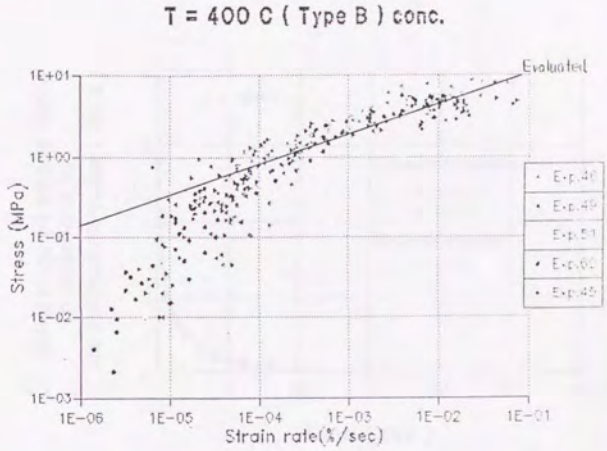

Figure 5.3.2.6 : Over stress behavior by Chaboche's model compared with experimental data
T = 400℃ (hold strain value = 0.4%)

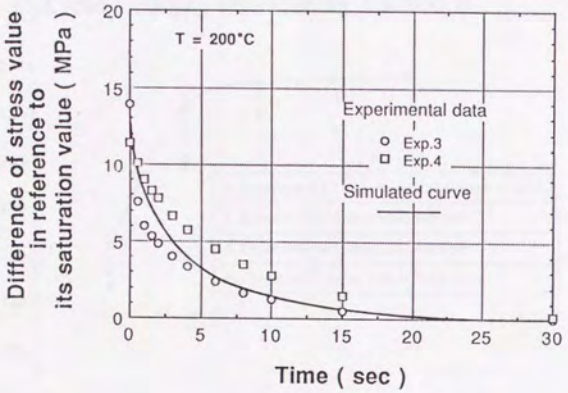

Figure 5.3.2.7 : Relaxation behavior by Chaboche's model compared with experimental curve for T = 200℃
(hold strain value = 0.4 % after cyclic test with $\Delta\varepsilon$ = 0.4 %, $\dot{\varepsilon} = 2.0\times10^{-4}$/sec)

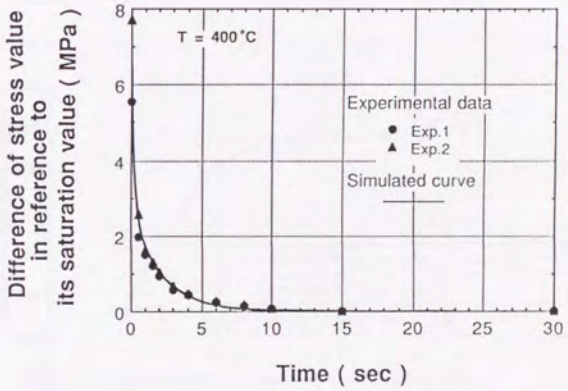

Figure 5.3.2.8 : Relaxation behavior by Chaboche's model compared with experimental curve for T = 400℃
(hold strain value = 0.4 % after cyclic test with $\Delta\varepsilon$ = 0.4 %, $\dot{\varepsilon} = 2.0\times10^{-4}$/sec)

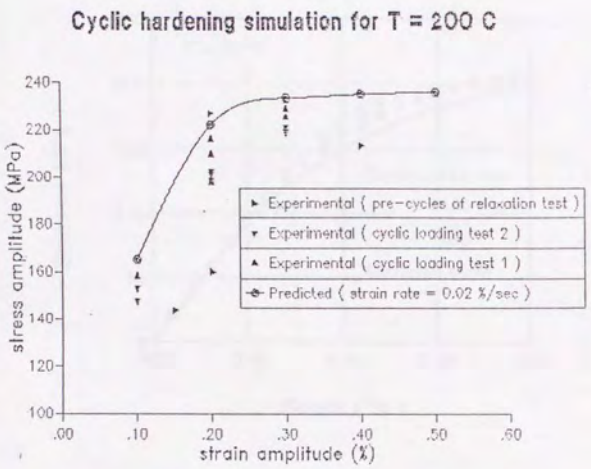

Figure 5.3.2.9 : Cyclic hardening behavior by Chaboche's model compared with experimental curve for T = 200℃
($\Delta\varepsilon = 0.4\ \%$, $\dot{\varepsilon} = 2.0 \times 10^{-4}$/sec)

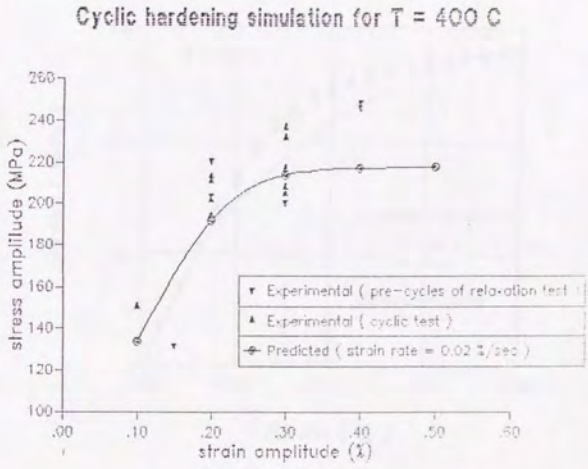

Figure 5.3.2.10 : Cyclic hardening behavior by Chaboche's model compared with experimental curve for T = 400℃
($\Delta\varepsilon = 0.4\ \%$, $\dot{\varepsilon} = 2.0 \times 10^{-4}$/sec)

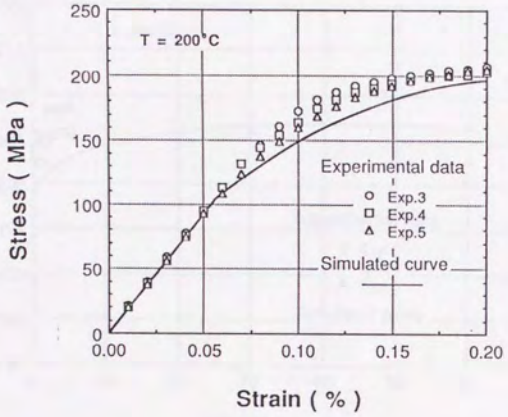

Figure 5.3.3.1 : Tensile behavior by Chaboche's model compared with experimental curve for T = 200℃
($\Delta\varepsilon = 0.4\ \%, \dot{\varepsilon} = 2.0 \times 10^{-4}$/sec)

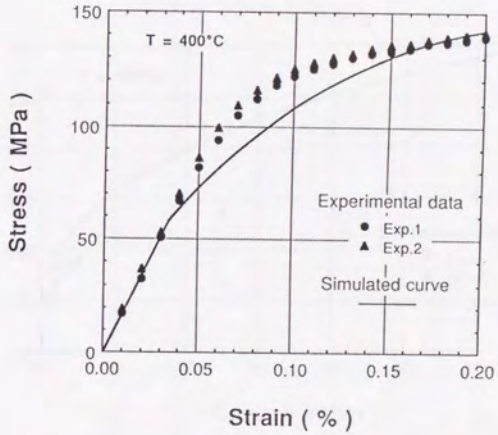

Figure 5.3.3.2 : Tensile behavior by Chaboche's model compared with experimental curve for T = 400℃
($\Delta\varepsilon = 0.4\ \%, \dot{\varepsilon} = 2.0 \times 10^{-4}$/sec)

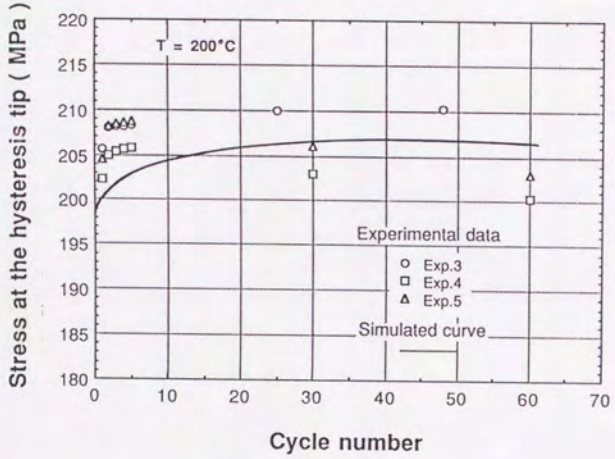

Figure 5.3.3.3 : Hardening behavior by Chaboche's model compared with experimental curve for T = 200℃
($\Delta\varepsilon$ = 0.4 %, $\dot{\varepsilon} = 2.0\times10^{-4}$/sec)

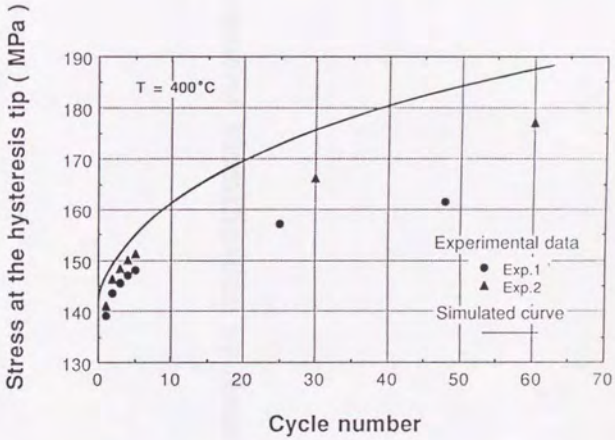

Figure 5.3.3.4 : Hardening behavior by Chaboche's model compared with experimental curve for T = 400℃
($\Delta\varepsilon$ = 0.4 %, $\dot{\varepsilon} = 2.0\times10^{-4}$/sec)

6 Parameter Identification by Neural Network

6.1 Objectives of Application of the Neural Network

As mentioned in the previous chapter, the numerical parameter evaluation procedures refer the cyclic, relaxation, hardening and tensile behaviors iteratively and repeatedly to evaluate stepwise the acceptable parameter values of K, n, H, D, h, d and k as a parameter set, while the behavior reference and the parameter evaluation are not carried out at the same moment. Using the neural network, these material behaviors and parameter values can be referred as the input data and the output data, respectively. If it is of importance to refer these material data concurrently with parameter values, the neural network is better desirable.

In this chapter, the neural network is applied to evaluate the parameters included in the uniaxial form of Chaboche's viscoplastic equations. The objective is not to get the exact parameter values mathematically, but to find out the most appropriate parameter set with respect to the various material behaviors.

6.2 Principles of the Hierarchical Neural Network

6.2.1 Theoretical Overview of the Hierarchical Neural Network

The neural network with the more number of connections among units can predict complicated relationships the more accurately as the brain with the more number of synapses among neurons can carry out the more difficult works. The neural network may be graded up with the more number of connections among units, and the more number of layers or units in a layer may provide with the more number of connections.

The simplest hierarchical network as shown in Figure 6.2.1.1 has only one input and one output layer which is called " a two-layered neural network " or" a flat neural network ". The reflection Y of the output unit shown in the figure is led from equation 6.2.1.1 with weights w_1 and w_2, input values x_1 and x_2, a sigmoid activation function f and an off-set value g.

$$Y = f(x_1w_1 + x_2w_2 + g) \qquad (6.2.1.1)$$

A sigmoid function (or a sigmoid activation function) is defined as follows whose curve is shown in Figure 6.2.1.2 :

$$f(x) = \frac{1}{1 + \exp(\frac{-2x}{u_o})} - n_o \qquad (6.2.1.2)$$

where u_o and n_o are function parameters corresponding to the steepness of the function curve at the center domain and to the center value, respectively. The parameter u_o is called " temperature " of the function. This function is convenient because its differential form may be expressed in terms of the original form as follows, which helps its training category by means of simple computation :

$$f'(x) = 2 [f(x) + n_o] \frac{1 - f(x) + n_o}{u_o} \qquad (6.2.1.3)$$

Then, equation 6.2.1.1 suggests that function f divides the (x_1,x_2) plane into two parts as shown in Figure 6.2.1.3. If the temperature u_o increases, the steepness of the border line gets gentle. If the number of input units increases to be j, the (x_1, ... ,x_j) space (a j-dimensional space) is taken into consideration.

Except for an input layer or an output layer, some networks which are expected to learn a more complicated relationship have one or more hidden layers. Three-layered neural network as shown in Figure 6.2.1.4 is normally used because of its rather simple construction. The final reflection Y_{fin} which is obtained from the output unit shown in the figure is the compound action of the reflections of two units Y_1 and Y_2 in the hidden layer. Therefore, Y_{fin} suggests that the (x_1,x_2) space is divided into two parts as shown in Figure 6.2.1.5. Furthermore, the k-layered neural network with j input units can divide the j-dimensional plane into two regions by means of k lines.

6.2.2 Back Propagation

Back propagation is a supervised training method, where all weights and off-set values are calculated and adjusted to make the total output error the minimum throughout training category. The determination of the weights and the off-set values is led by the following equations. In this section, a three-layered neural network is considered as an example and its training category based on back propagation is discussed.

Back propagation can be stated to consist of four steps as follows:

Step-1 ; All the hidden layered units make each output layer unit calculate the output value O_{kp} corresponding to training pattern p as follows:

$$O_{kp} = f(S_{kp}) \qquad (6.2.2.1)$$

$$S_{kp} = \sum_j (V_{kj} H_{jp} + g_k) \qquad (6.2.2.2)$$

where S_{kp} is called the internal potential of output unit k corresponding to training pattern p, V_{kj} is the weight between hidden unit j and output unit k, and H_{jp} and g_k are an input value from hidden unit j and an off-set value for output unit k, respectively. A function f is a sigmoid activation function as introduced in the last section.

Step-2 ; At the first stage, the calculated output value O_{kp} of each output unit is not correct. Then, the value should be compared with the target value T_{kp} to calculate the square-error D_p as follows:

$$D_p = \frac{\sum_k (T_{kp} - O_{kp})^2}{2} \qquad (6.2.2.3)$$

The square-error D_p corresponds to the distance from the real value and should decrease to zero for the correct output. Its differential with respect to weight V_{kj} is expressed as follows:

$$\frac{\delta D_{kp}}{\delta V_{kj}} = \frac{\delta D_{kp}}{\delta O_{kp}} \frac{\delta O_{kp}}{\delta V_{kj}}$$

$$= [- (T_{kp} - O_{kp})] f' (S_{kp}) H_{jp}$$

$$= - (T_{kp} - O_{kp}) b_1 O_{kp} (1 - O_{kp}) H_{jp} \qquad (6.2.2.4)$$

where f' is the derivative of the function f with respect to S_{kp}, and b_1 is a constant.

Step-3 ; Based on a gradient decent method which is one of the least mean square methods, the incremental value of each weight V_{kj} can therefore be determined by moving along the steepest slope of the error surface as follows:

$$\Delta V_{kj} = b_2 (T_{kp} - O_{kp}) O_{kp} (1 - O_{kp}) H_{jp} \qquad (6.2.2.5a)$$

After each training pattern, weights are adjusted. On the other hand, if weights are expected to be adjusted after all the training patterns, the incremental value of each weight V_{kj} can be determined by the following expression :

$$\Delta V_{kj} = \sum_p b_{2p} (T_{kp} - O_{kp}) O_{kp} (1 - O_{kp}) H_{jp} \qquad (6.2.2.5b)$$

where, b_2 and b_{2p} are constants. In the same way, the incremental value of each off-set g_k is also determined with a constant d_2 or d_{2p} as follows:

$$\Delta g_k = d_2 (T_{kp} - O_{kp}) O_{kp} (1 - O_{kp}) \qquad (6.2.2.6a)$$

or

$$\Delta g_k = \sum_p d_{2p} (T_{kp} - O_{kp}) O_{kp} (1 - O_{kp}) \qquad (6.2.2.6b)$$

while an off-set term can be regarded as the zero-series of H_{ip}.

Step-4 ; Computational scheme for the range of adjusting each weight between an input unit and a hidden unit and an off-set value of each hidden unit is the same as the above mentioned schemes. Finally, the following adjustment range can be obtained for weights :

$$\Delta W_{ji} = b_4 E_p V_{kj} H_{jp} (1 - H_{jp}) I_{ip} \qquad (6.2.2.7a)$$

or

$$\Delta W_{ji} = \sum_p b_{4p} E_p V_{kj} H_{jp} (1 - H_{jp}) I_{ip} \qquad (6.2.2.7b)$$

and for off-set values :

$$\Delta h_j = d_4 E_p V_{kj} H_{jp} (1 - H_{jp}) \qquad (6.2.2.8a)$$

or

$$\Delta h_j = \sum_p d_{4p} E_p V_{kj} H_{jp} (1 - H_{jp}) \qquad (6.2.2.8b)$$

where I_{ip} is the input value of input unit i corresponding to pattern p, and b_4, b_{4p}, d_4 and d_{4p} are constants. A variable E_p is defined in equation (6.2.2.9), such that

$$E_p = \sum_k (T_{kp} - O_{kp}) O_{kp} (1 - O_{kp}) \qquad (6.2.2.9)$$

With the gradient decent method, minor misjudgement where the training stops at the local minimal point of the square error exists, while a few time trials of adjusting the initial values of weights and off-sets lead to the real minimum point of the square error.

6.2.3 Employed Neural Network

Generally, a three-layered neural network with sufficient number of units is known to map almost every relationship without mathematical proof. Furthermore, the learning time rapidly increases with more than four layers. Therefore, in the present studies, three-layered neural network is taken into consideration. The number of units in each layer, that is an input layer, a hidden layer and an output layer, is not fixed. The sigmoid function employed is expressed for each unit i as follows :

$$O_i = \frac{1}{1 + \exp(- S_i)} - 0.5 \qquad (6.2.3.1)$$

where constants n_o and u_o are defined such that

$$u_o = 2$$

and

$$n_o = 0.5$$

and S_i is the internal potential which will be explained later. Its configuration is shown in Figure 6.2.3.1. Activation O_i as the reflection of unit i should be in the range of -0.5 to +0.5.

Reformed back propagation is employed for the network training. Through the method, weights and off-set values are adjusted in the following manner based on the back propagation :

$$\Delta V'_{kj} = a_v \Delta V_{kj} + b_v \underline{\Delta V_{kj}} \qquad (6.2.3.2)$$

$$\Delta W'_{ji} = a_w \Delta W_{ji} + b_w \underline{\Delta W_{ji}} \qquad (6.2.3.3)$$

$$\Delta g'_k = a_g \Delta g_k + b_g \underline{\Delta g_k} \qquad (6.2.3.4)$$

$$\Delta h'_j = a_h \Delta h_j + b_h \underline{\Delta h_j} \qquad (6.2.3.5)$$

Here, the prime notations on weights and off-set values appeared on the left sides and the underlined terms on the right sides of the above expressions correspond to the currently employed range of adjustment and that in the previous trial (training cycle), respectively. Terms without notations correspond to the calculated range by the back propagation. Neural parameters a_o and b_o

(where subscript o = v, w, g or h) are called a learning rate and a momentum term, respectively. Learning rate suggests how rapidly weight or off-set values should be adjusted, and a momentum term does how much the history of the previous adjustments should be referred. These neural parameters should be determined depending on situations, for examples, which relationship it should map, and how much the square error is. In this network, the learning rate and the momentum term can be set for each layer.

The total error function E_{total} is the sum of all the square-errors of output units for all the patterns expressed as follows:

$$E^2_{total} = \frac{\sum_p \sum_k (T_{kp} - O_{kp})^2}{N_p \times N_k} \qquad (6.2.3.6)$$

where N_p and N_k are the number of the patterns and the output units, respectively. After some iterations of training cycles, the weights and the off-set values are saturated to predict the correct output values with negligibly small value of the total error function E_{total}. Then, the network which has these values of weights and off-sets can evaluate the aiming relationship well if the numbers of the training patterns, the input units and the units in the hidden layer are sufficient.

6.3 Identification Procedures and Results

6.3.1 Training Procedure

In the application of a neural network to evaluate the parameter set included in the uniaxial and stationary temperature form of Chaboche's constitutive equations, the input and the output values should be determined as follows :

Input values ; The various material behaviors were inputted to the input units as I_{ip}.

output values ; The corresponding parameter set of seven parameters K, n, H, D, h, d and k were outputted from the output units as O_{kp}, where the value of k must be 1 to 7.

As the input values, such material behaviors as a tensile curve, a cyclic hysteresis loop, a cyclic strain hardening curve and a relaxation curve of the cyclic and the succeeding relaxation tests were employed. The strain conditions such as strain range of $\Delta\varepsilon = 0.4\%$ and strain rate of $\dot{\varepsilon} =$

2.0×10^{-4} /sec were fixed. The referred cycle number was the sixtieth cycle of the cyclic tests (or simulations).

Training procedures were carried out for both temperature cases of T = 200℃ and 400℃ independently. (Therefore, two different neural networks were made up for these temperature cases.) Through the training procedure, the pattern sets of the input and output data were made by the numerical simulation explained in Chapter 3. As shown in Figures 6.3.1.1 to 6.3.1.4, eleven units, twenty-one units, eight units and ten units corresponding to a tensile behavior, a cyclic loop, a hardening behavior and a relaxation behavior were finally prepared after some preliminary trials. The additional training patterns were chosen with the reference of the parameter identification results by means of the numerical procedures described in Chapter 5, which help to evaluate more accurate parameter sets.

6.3.2 Values of the Evaluated Parameters

After pattern learning, the parameter sets corresponding to the experimental input data came out for temperature conditions of T = 200℃ and 400℃. As the input data, cyclic tests of V07 to V13 and relaxation tests of R06 to R15 were employed and the average of the experimental curves on stress value for the both temperature cases were finally inputted. With these parameter sets, tensile curves, cyclic hysteresis curves, cyclic strain hardening curves and relaxation curves were simulated and were compared with the corresponding experimental data.

The obtained parameter sets are shown in Table 6.3.2.1 for each temperature value. Since the neural network decides the same output values from the same input data, no need (no possibility) for choosing the best parameter set among some candidate sets exists on the contrary to the previously mentioned method.

6.3.3 Comparison between Fitted and Experimental Curves

Cyclic loading simulations and relaxation simulations by Chaboche's model with these parameter sets are shown in this section with the corresponding experimental data for each temperature value, respectively. These behaviors were directly referred to fit the parameters to them.

For cyclic behaviors, Figures 6.3.3.1 and 6.3.3.2 show the saturated cyclic hysteresis curves for temperature cases of T = 200℃ and 400℃ with strain range of $\Delta\varepsilon = 0.4\%$, which were simulated by Chaboche's model with the evaluated parameter sets. Slight disagreement of 7% (in the case of T = 200℃) to 12% (in the case of T = 400℃) at the hysteresis tips (both at the maximum and the minimum stress points) is smaller than that of over 15% in the previous studies. The confirmation of the hysteresis loops satisfies good agreement on the curvature between the

experimental and the simulated curves.

As to relaxation behaviors, Figures 6.3.3.3 and 6.3.3.4 show the relaxation curves for two temperature cases, which were simulated by Chaboche's model with the evaluated parameter sets. The simulated curve for temperature of T = 200℃ runs within the experimental data scattering, while that for T = 400℃ does not run within the scattering.

As to tensile behaviors, Figures 6.3.3.5 and 6.3.3.6 show the comparison between the simulated curves by Chaboche's model and the experimental curves for two temperature cases, respectively. While the simulated curves run just in the scattering of the experimental data, the stress values at the strain value of 0.2% on these curves are greater than the experimental values.

As to cyclic strain hardening behaviors, Figures 6.3.3.7 and 6.3.3.8 show the comparison between the simulated curves by Chaboche's model and the experimental curves for two temperature cases, respectively. In both temperature cases, the curves run just within the experimental data, which suggests that the simulated curves are accurate.

Table 6.3.2.1 : Evaluated results for two temperature cases

Temperature	K	n	H	D
200℃	1.02×10^{2}	3.76	1.34×10^{5}	1.39×10^{3}
400℃	1.21×10^{2}	2.89	1.12×10^{5}	1.30×10^{3}

Temperature	h	d	k
200℃	1.85×10^{2}	1.38	1.22×10^{2}
400℃	4.92×10^{2}	4.18	0.72×10^{2}

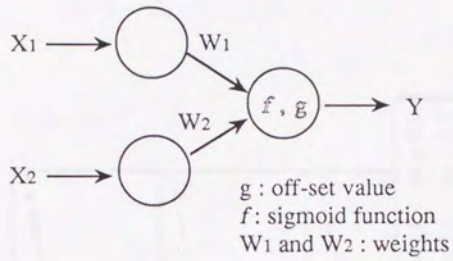

Figure 6.2.1.1 : Neural network with two input units and one output unit

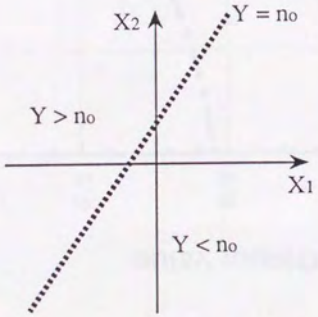

Border line Y = no is obtained from function *f*, off-set value g and weights

Figure 6.2.1.3 : Division of (X1,X2) plane by two-layered neural network

Figure 6.2.1.2 : Documents by a Sigmoid Function

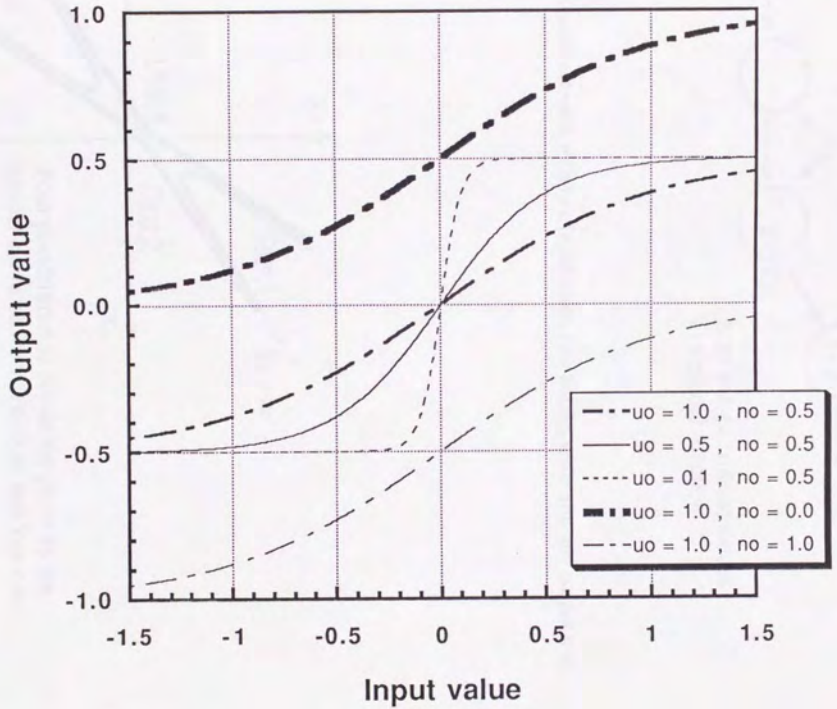

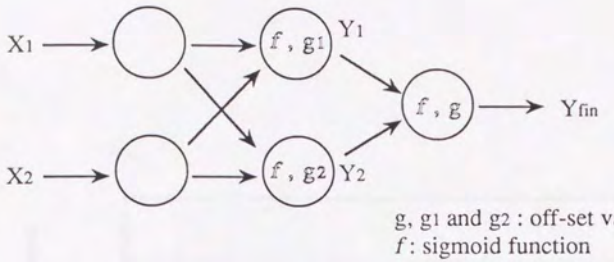

Figure 6.2.1.4 : Neural network with two input units, two hidden units and one output unit

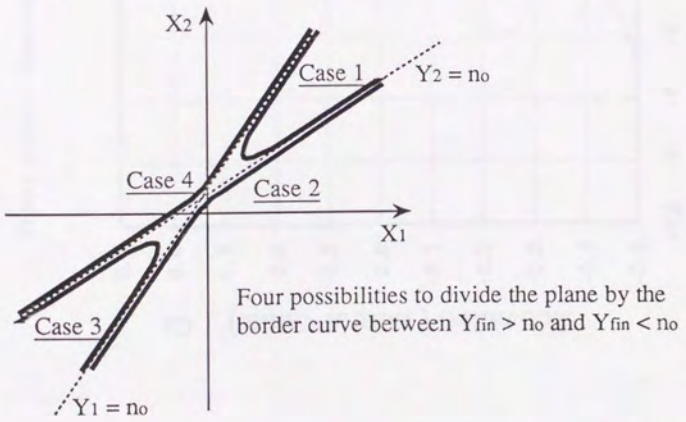

Figure 6.2.1.5 : Division of (X1,X2) plane by three-layered neural network

Figure 6.2.3.1 : Document by an employed sigmoid function

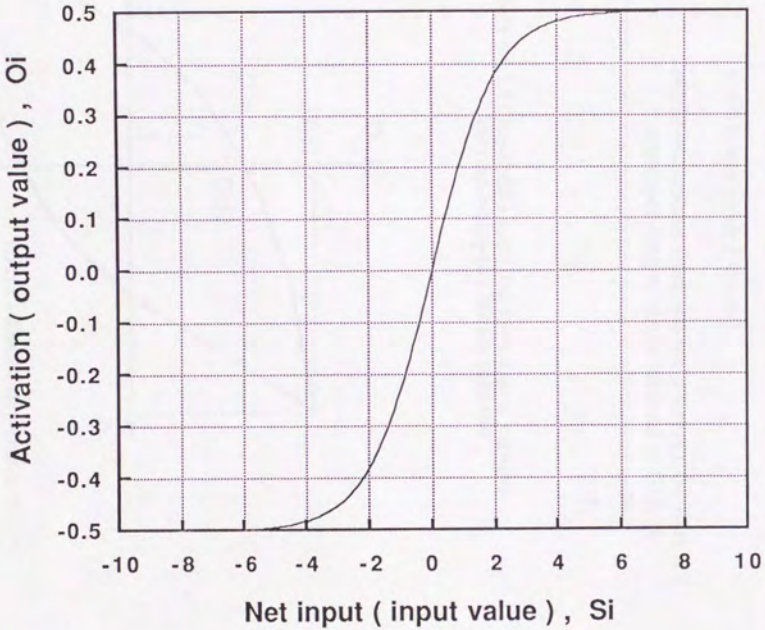

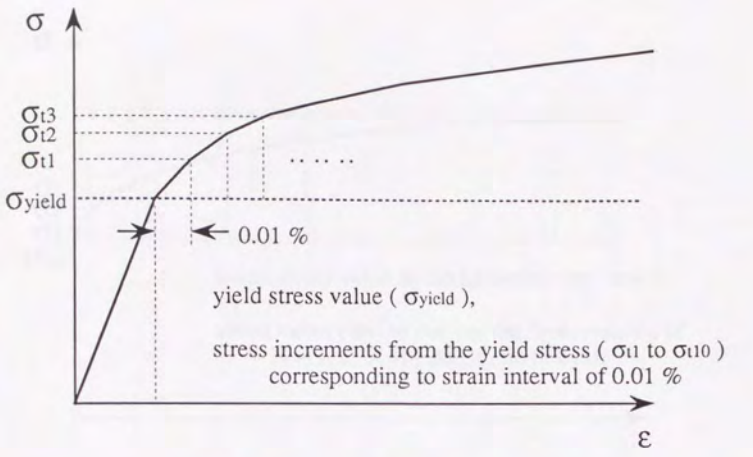

Figure 6.3.1.1 : Input data sampling for a neural network corresponding to a tensile behavior

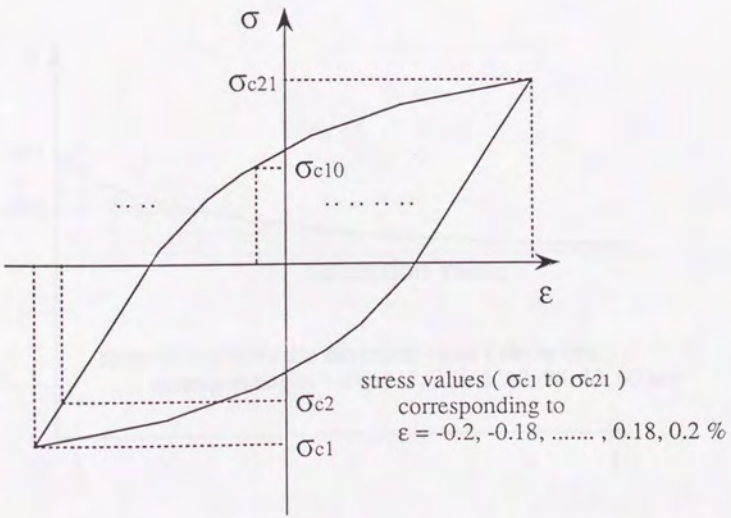

Figure 6.3.1.2 : Input data sampling for a neural network corresponding to a cyclic behavior

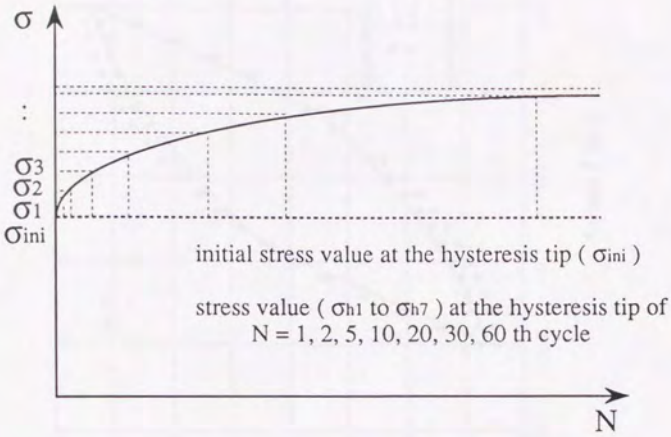

Figure 6.3.1.3 : Input data sampling for a neural network corresponding to a hardening behavior

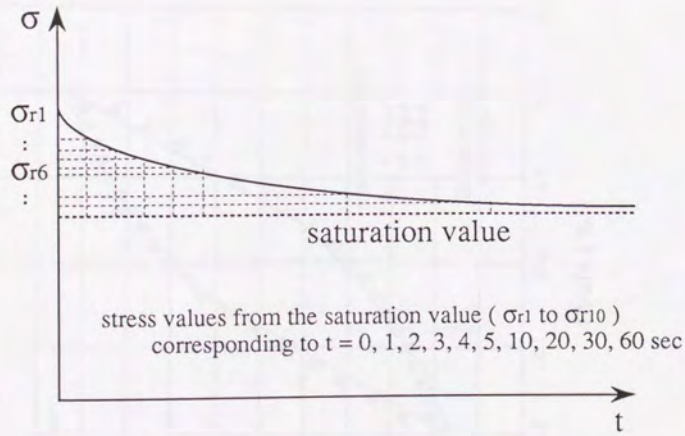

Figure 6.3.1.4 : Input data sampling for a neural network corresponding to a relaxation behavior

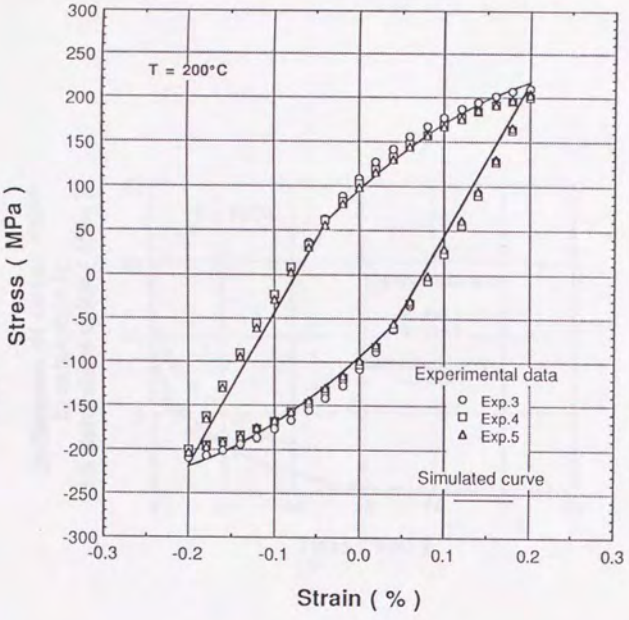

Figure 6.3.3.1 : Cyclic behavior by Chaboche's model compared with experimental curve for T = 200℃

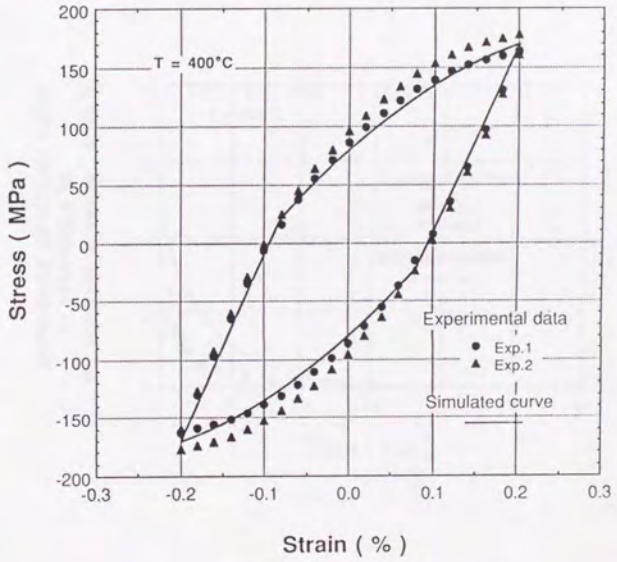

Figure 6.3.3.2 : Cyclic behavior by Chaboche's model compared with experimental curve for T = 400℃

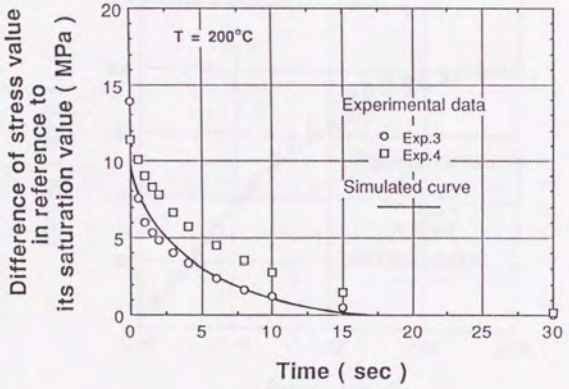

Figure 6.3.3.3 : Relaxation behavior by Chaboche's model compared with experimental curve for T = 200℃

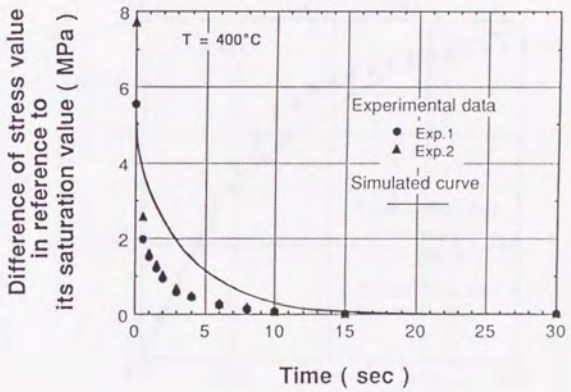

Figure 6.3.3.4 : Relaxation behavior by Chaboche's model compared with experimental curve for T = 400℃

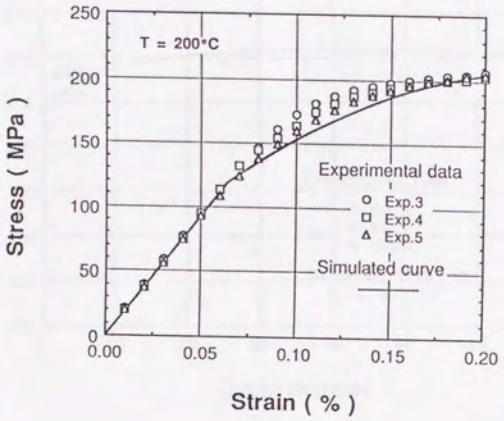

Figure 6.3.3.5 : Tensile behavior by Chaboche's model compared with experimental curve for T = 200℃

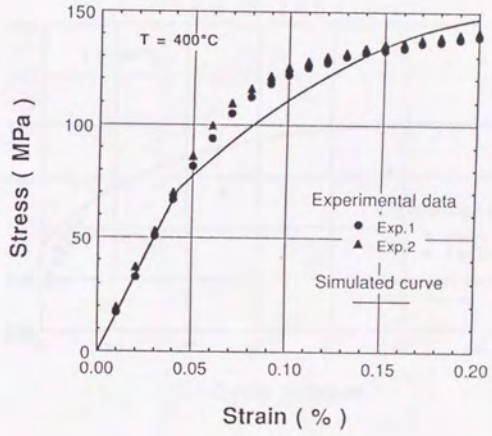

Figure 6.3.3.6 : Tensile behavior by Chaboche's model compared with experimental curve for T = 400℃

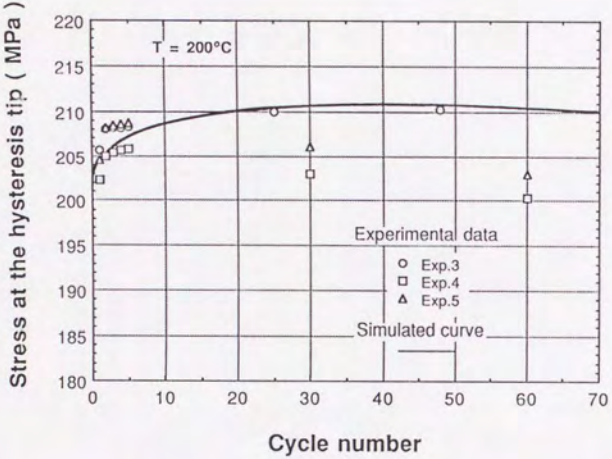

Figure 6.3.3.7 : Hardening behavior by Chaboche's model compared with experimental curve for T = 200℃

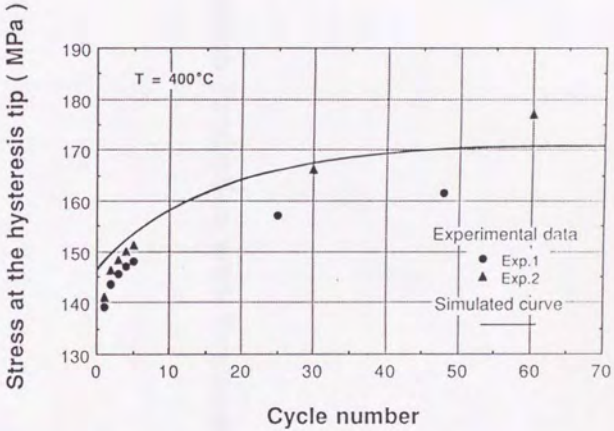

Figure 6.3.3.8 : Hardening behavior by Chaboche's model compared with experimental curve for T = 400℃

7 Lifetime Prediction with Evaluated Parameters

7.1 Outline and Objectives

In this chapter, the lifetime of the first wall is calculated based on the fatigue laws with the uniaxial and stationary temperature model of Chaboche's constitutive equations. The boundary conditions were considered such that only thermal conditions exist and neither external mechanical loading nor irradiation effects were taken into consideration. The viscoplastic model given in equations 3.1.3.1 to 3.1.3.4 with the parameter sets obtained for different temperatures by the numerical identification method which was described in chapter 5, has been implemented in the ABAQUS FE-code (Ref. [7.1]). An IBM computer was employed and the implementation of the viscoplastic model in the computer program was worked out by Nuclear Research Center Karlsruhe.

The objective is to confirm the difference in the prediction results caused by the employed models. The ORNL theory (Ref. [7.2]), which is based on a flow rule that shows linear kinematic and isotropic hardening, and a simple plasticity model, which includes linear isotropic hardening, have also been used to determine stress-strain fields for comparison. The employed bilinear curves describing saturation cyclic are included in Figures 7.1.1 and 7.1.2.

7.2 FE-Analysis Method

7.2.1 Calculation Area

A cross-section of a typical first wall design is depicted in Figure 7.2.1.1 and the marked section is the area to be taken into analyses. The FE-mesh shown in Figure 7.2.1.2 consists of 228 two-dimensional elements with 773 nodes. Each element has 8 nodes.

7.2.2 Thermal Analyses

The details of the various heat conditions on the first wall have been described in Chapter 2. In this chapter, following the fusion program of the European Community, these specimens are being examined for fatigue under thermo-mechanical conditions that are close to the loading of " a next generation's fusion machine " being in the preliminary design by European Community.

The maximum surface heat flux of 40 W/cm^2, the maximum volumetric heat deposition of 14 W/cm^3 and the internal heat generation due to neutron fluency were considered in thermal analyses. The thermo-mechanical cycles are characterized by burn time of 500 sec and off-burn time, shut down plus dwell time of 260 sec. Figures 7.2.2.1 and 7.2.2.2 show the heat conditions and the operation history, respectively.

7.2.3 Mechanical Analyses

In mechanical analyses, generalized plane strain (normal to the plane of the fatigue) has been considered to be the most suitable boundary condition. The fatigue behavior of the structure is described by the cyclic variation in stress and strain. In this analyses, the boundary condition is as shown in Figure 7.2.3.1.

In the first analysis, stress-strain fields were calculated utilizing the ORNL model, which needed just two cycles to simulate the whole cyclic domain until the saturation of the specimen. Since no further creep-plasticity interaction was taken into consideration in the analyses, the second thermal period induced a saturated stress-strain cycle.

Moreover, Chaboche's model has been applied to the analysis. As it is not realistic to calculate stress and strain for several hundred cycles to reach the saturation, the procedure is split up into two steps.
1st step : A small number of cycles (in the present analyses, four cycles) were calculated with periodic loading until "first-cycle saturation" in the peak stress and strain levels (hysteresis tip) was reached with a small amount of isotropic hardening. The last stage of this step (in the present analyses, the forth cycle) suggests the expected saturated stress components of back stress and over stress.
2nd step : The isotropic hardening variable (yield stress) R was fixed to be its saturation value R_s and on the basis of the fields obtained in the first step, an analysis with a small number of cycles (in the present analyses, five cycles) is performed to reach the stable stress-strain cycles. The last stage of this step (in the present analyses, the fifth cycle) suggests the expected saturated hysteresis curve.

7.3.1 Stress-Strain Fields

At first sight, the calculated results look rather similar to both material models used. In Figures 7.3.1.1 and 7.3.1.2, contour plots of the axial stress are traced for both material models. The diagrams show the behaviors at the end of heating and at the end of dwell time. The maximum values of tensile and compressive stresses differ by up to 10 %. The extreme values, however, do not occur at the same locations of the structure.

Due to the non-linear hardening rule of Chaboche's model, stress and strain redistributions take place over a large number of cycles. For example, at the most exposed location (which is at the heated front surface), the plastic strain range is continuously reduced in terms of time. Starting at a value of 0.408% (the first cycle), it decreases down to 0.362% (the third cycle) and finally reaches to 0.321% within a saturated hysteresis loop.

For a stable cycle, the mechanical equivalent strain range is calculated to be 0.590%. For comparison, the ORNL model predicts 0.568%, and a simple plasticity model yields 0.433% of the mechanical strain range. Taking into account the fatigue curves given in the RCC-code (Ref. [7.3]) the lifetime of the component can be assessed.

7.3.2 Lifetime

Depending on the individual material model, the number of cycles up to the crack initiation are predicted to be 2690 by Chaboche's model, 3030 by ORNL model and 7780 by plasticity model, respectively. Chaboche's model suggests the most severe case, while these predicted results should be confirmed by experimental tests.

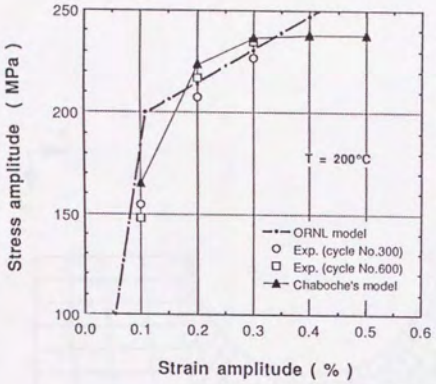

Figure 7.1.1 : Employed bilinear curves compared with experimental data and curve by Chaboche's model (T = 200℃)

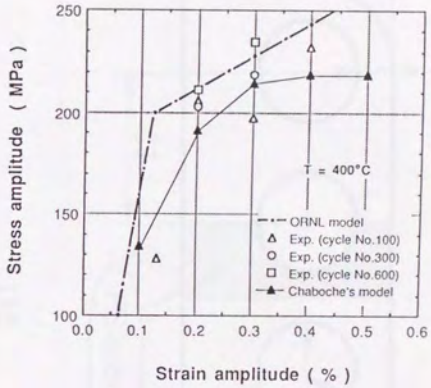

Figure 7.1.2 : Employed bilinear curves compared with experimental data and curve by Chaboche's model (T = 400℃)

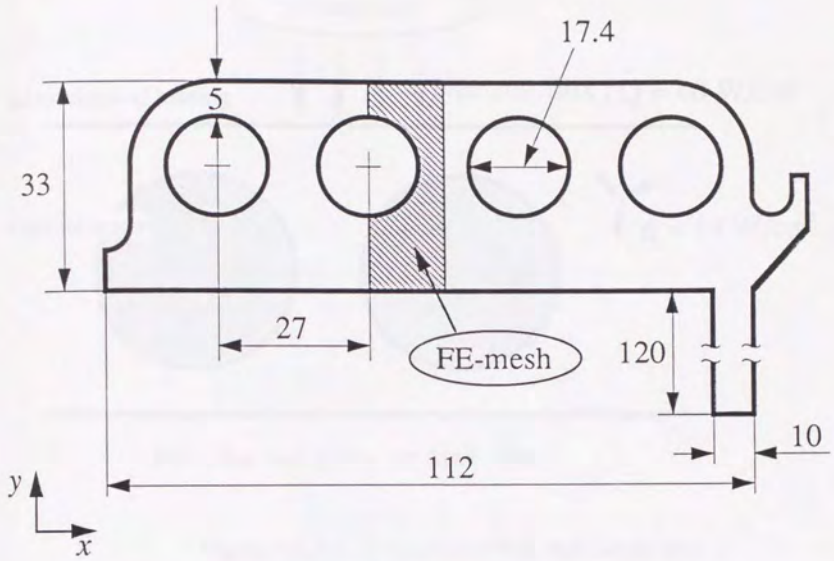

Figure 7.2.1.1 : A cross-section of a typical first wall design

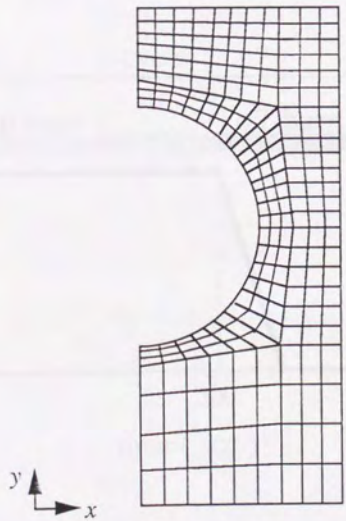

Figure 7.2.1.2 : Employed FE-mesh

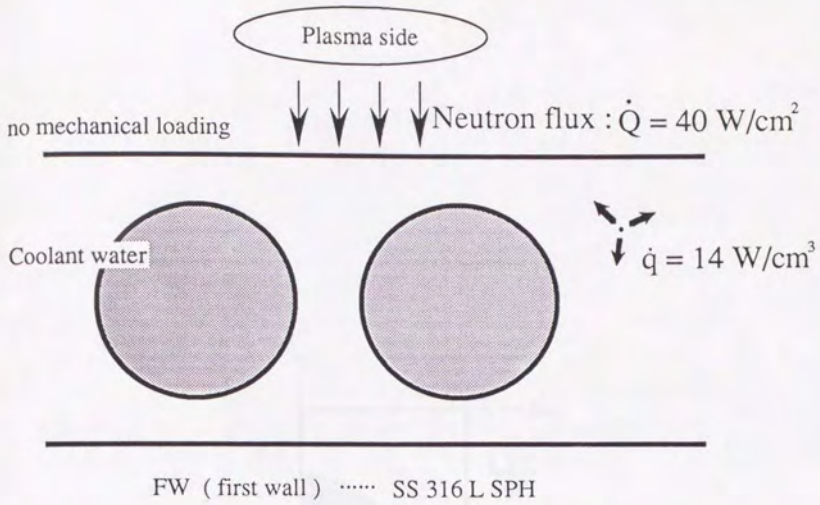

Figure 7.2.2.1 : Considered first wall conditions

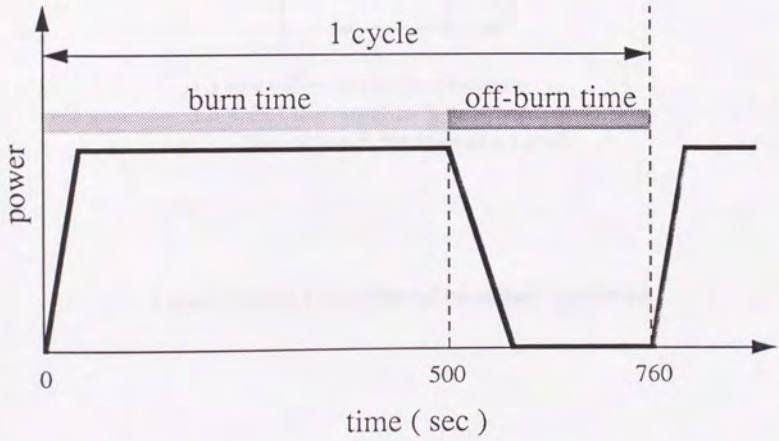

Figure 7.2.2.2 : Considered burning history

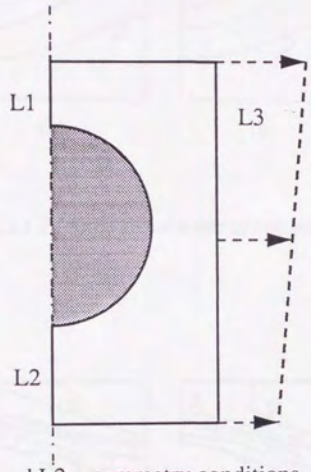

Figure 7.2.3.1 : Considered boundary condition

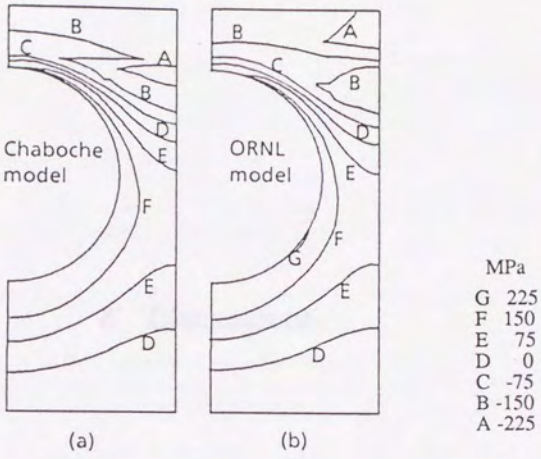

Figure 7.3.1.1 : Axial stress fields at end of heating

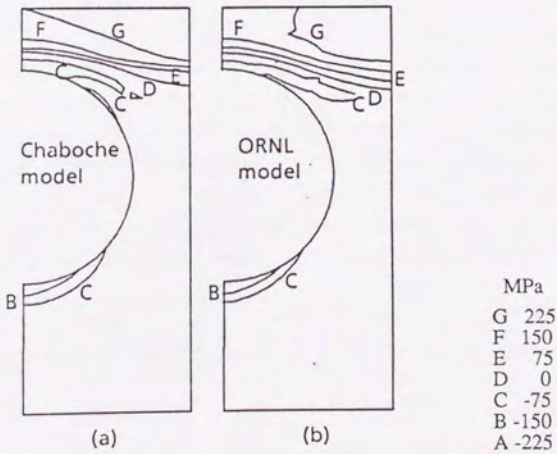

Figure 7.3.1.2 : Axial stress fields at end of cycle

8 Discussions

8.1 Application Suitability of Chaboche's model to the First Wall Material

8.1.1 Theoretical Incompleteness of Chaboche's Model

The employed Chaboche's viscoplastic theory can well explain the cyclic behavior during a wide range of inelastic strain domain with taking two hardening parameters Y and R into consideration while the theory can not well explain some other behaviors. In this sub-section, the main problems involved in Chaboche's model related with the present studies are described.

Chaboche's theory is not so suitable to explain the simple tensile behavior. In fact, the stress increment simulated by Chaboche's model decreases just at the border between the elastic and the inelastic domains (i.e., at the initial yielding point), while the distinctive border between the elastic and the inelastic domains is not observed in the experimental simple tensile curves. At the border point, the inelastic strain value ε^p simulated by Chaboche's model suddenly starts increasing from its initial value of zero and the inelastic strain rate $\dot{\varepsilon}^p$ skips discontinuously from zero to a certain value over zero when the stress value increases over the yield stress value σ_y. Therefore, the smooth configuration of the material behavior curve which stainless steel, for example SS 316L SPH, shows can not be well drawn by Chaboche's model without exhibiting a certain bending point on the tensile curve. When this model is employed to explain the fatigue phenomena, attention should be paid to confirm which domain is plastic in the fatigue loading cycles, i.e., the difference in the strain values between the predicted by this model and the actually measured is very important. This problem may occur when any model which includes the yield function is employed. On the other hand, a bending between the elastic and the inelastic domains on the cyclic curve, which Chaboche's model draws, is not so large and the cyclic behavior can be rather well fitted with simulations using Chaboche's constitutive equations.

No aging effect can be explained by Chaboche's theory. Miller and Robel tried to include an aging term in their theories.

Especially on stainless steel, slower strain rate $\dot{\varepsilon}$ can sometimes actually lead higher stress σ. During a cyclic loading test, the shift down of strain rate in the way shown in Figure 8.1.1.1, makes a higher value of stress at the hysteresis tip as shown in Figure 8.1.1.2. This fact can not be explained by Chaboche's theory. Here, a certain relationship between stress σ and strain rate ε can be searched as shown in Figure 8.1.1.3, which suggests a non-linear relationship in real metallic

materials. The problem is which of a linear or a non-linear approximation on σ-ε relationship is more suitable to describe the actual behaviors.

Application of Chaboche's theory to thermal fatigue causes some problems due to various temperature conditions. For an example, parameters H and h should be described as functions of temperature, and the following correlation is sometimes used instead of relation 3.1.3.3 under a uniaxial condition :

$$\dot{Y} = H(T)\,\dot{\varepsilon}^{p} - D\,Y\left|\dot{\varepsilon}^{p}\right| + \frac{\partial H}{\partial T}\frac{1}{H}\,Y\,\dot{T} \qquad (8.1.1.1)$$

Actually, Figure 8.1.1.4 was obtained from experiments.

8.1.2 Suitability of the Application to Cyclic Behavior on the First Wall

It is of importance to evaluate the parameter set satisfying the physical significances with not only cyclic behaviors but other experimental behaviors, since for an example a hardening history gives rather large influence to the stress history after many cycles. The most important point here is that the employed Chaboche's model does not completely describe all the viscoplastic material behaviors. If the model is perfect, it can be chosen to determine the parameter set which is fitted to all the cyclic loops from the first to the saturated, though it is, however, impossible and has no sense. For the lifetime prediction by means of FE calculation, the cyclic loops nearly after the saturation and the stress histories at the hysteresis tip from the beginning are quite important to be fitted. In the present studies, therefore, the parameter evaluation was carried out with reference to these experimental data.

On the saturated cyclic hysteresis curves for temperature cases of T = 200℃ and 400℃, the curvature of the loop could be well fitted, and the stress value of the hysteresis tip could be simulated within the discrepancy of 4 to 12 % from the experimental values by Chaboche's model. On the configuration of the simulated cyclic hysteresis curves, the border point between the elastic and the inelastic domains is obvious but does not show such big bending. For the hardening behavior, the simulated curves are quite similar to the experimental curves, which suggests confidence to predict the reasonable lifetime with the evaluated parameter sets. The fitting error of 4 to 12 % can be considerably good compared with the results reported in the previous studies of over 15 %. The employed Chaboche's model can be regarded as one of the suitable viscoplastic evaluation models for the first wall of a fusion reactor.

The parameter evaluation results both by a numerical identification method and a neural identification method show that the accurate parameter evaluation for temperature case of T = 400℃ is somehow more difficult than that for T = 200℃. It is not clear but may be that the real first wall behavior under the cyclic operation condition is departed from that exhibited by

Chaboche's model under high temperature (of T = 400℃). The simple modeling of hardening with parameters Y and R in the constitutive equations may be the reason. At high temperature condition, the employed stainless steel SS 316L SPH shows larger hardening, so that it becomes more difficult for Chaboche's model to describe the behaviors under higher temperature. However, the departure can be regarded as small enough to apply the constitutive equations to the lifetime prediction of the first wall. By the way, the material scattering under higher temperature of T = 400℃ may be larger than that under the lower temperature.

8.2 Property of the Numerical identification Method

8.2.1 Advantages of the Method

If the parameter set was evaluated only from the experimental cyclic hysteresis curves, the disagreements (of 4 to 11 %) mentioned in the previous section would become smaller. However, Figures 5.3.2.7, 5.3.2.8, 5.3.2.9 and 5.3.2.10 show sufficient agreement between the experimental curves and the simulated ones, which supports as a whole that the obtained parameter sets are quite acceptable. In former studies, the parameters included in viscoplastic constitutive equations were determined one by one with reference to each individual experimental behavior independently such as, cyclic curves and creep curves. Therefore, the equations with the evaluated parameter set might not simulate all these experimental behaviors well. In the present studies, the reference experimental data include cyclic curves, relaxation curves and cyclic hardening curves, and the obtained parameter set should be satisfactory with respect to all these behaviors.

The basic idea to determine the parameter values is based on the least square algorithm. Using the numerical method, with referring a great number of experimental data, the numerically accurate results of parameter evaluation can be obtained. The numerical method gives the more accurate evaluation results while it needs the more time and work for repetitions.

The material scattering of the input experimental data can be reduced by sampling these various data instantaneously. The identification results will show the mean behavior within these experimental data scattering. Various experimental data can be just inputted to the evaluation of the parameter values as the relationship between the stress and the inelastic strain rate during the evaluation

procedures 1 and 3, while taking reference over these various data during the confirmation procedure 1 or 2 is difficult.

Chaboche's model has the temperature dependent parameters, while most of metallic material has temperature-dependent Young's modulus. In the presently developed numerical identification method, a value of Young's modulus being dependent on the temperature condition should be taken into consideration to calculate the elastic behaviors. Therefore, different values of Young's modulus for different temperature cases should be prepared before the parameter evaluation. The procedures are, however, available for each individual temperature case once the procedures have been so established, where the temperature-dependent Young's modulus is referred not directly but the simulated influence of each parameter to material behaviors is referred, which is carried out with Young's modulus affected a little by its temperature dependency.

8.2.2 Disadvantages of the Method

The method can well treat a great number of data from a few different types of experiments, while it can not well treat data from many different types of experiments. This is because the method has two confirmation procedures by manual operations.

The slight modification of the target parameter values during the confirmation procedures requests skill and experience on Chaboche's theory. Increase in the reference data number during the confirmation procedure needs also more time to repeat and more hard work with much skill for an evaluator. The iterating computation needs much amount of time, which can hardly be carried out on a small or a personal computer. The limited reference of the experimental data on which the currently evaluated parameters are based causes discrepancy in the parameter evaluation.

The establishment of a numerical identification method needs a great amount of time. For example, in the case that the mainly fitted behaviors (in the present studies, cyclic behaviors with different strain ranges), the employed viscoplastic model (in the present studies, Chaboche's model) or the reference experimental data during the confirmation procedures (in the present studies, cyclic hardening curves, cyclic hysteresis curves and hardening curves) should be changed, the flow of the identification procedures should also be changed from the beginning.

8.2.3 Further Comments on the Method

The method is more favorable if a viscoplastic constitutive equation is employed to be fitted to some experimental behaviors, where the number of the different types of experiments is only a few and certain limited types of behaviors are to be referred mainly, and where a great number of experimental data of the same type to be referred exist. In the present studies, cyclic behaviors for different temperature cases of T = 200℃ and 400℃ should be mainly fitted with Chaboche's

model. These behaviors are considered as the thermo-mechanical fatigue conditions on the first wall. With a main frame (IBM super computer), based on the numerically recorded experimental data of cyclic tests and succeeding relaxation tests, accurately evaluated parameter sets can be obtained within about fifty hours including the manual operations for the confirmation of parameter values with this tool. Before that, for the completion of the tool, some more days should be necessary. The reference data number of each cyclic hysteresis loop, each relaxation curve and stress value history at the hysteresis tip were about 120, 70 and over 60, respectively. As mentioned above, the identification method should employ a certain well-revealed behavior. The evaluation procedure needs much work with special skill and experience on the employed model and the reference behavior, but will be carried out accurately. If a viscoplastic model to be employed is unknown, the method can not be available. Establishment of the method is essentially not only for the pure tool of parameter determination but also of the theoretically important part to be studied.

In the present studies, parameters K and n are rather difficult to be discussed. For an example, insufficient number of reference experimental data (an insufficient data base) make a certain scattering in K and n, because these parameters K and n are not completely unique if they are determined from only a cyclic tests, and different pairs (K, n) can give nearly the same results of least-square fitting. This is an example which happened as a theoretical problem in the determination of the parameter set and should be solved during the design of the evaluation method.

It becomes more difficult to handle the parameter values during the confirmation procedures with referring the more various material behaviors, for examples, cyclic loops with different strain range or strain rate. The numerical identification method has a certain limit on the number of the various reference experimental data through the manual operations in confirmation procedures. On the other hand, all these various experimental data can be inputted as the relationships between inelastic strain rate and stress, and then a certain parameter set is evaluated. Here, the simulated behaviors by the evaluated parameter set is fitted to all the reference data. If some important behavior which should be fitted as completely as it can with respect to the attended material characteristics exists, the manual fitting is needed and the number of reference data which are not related strongly to the attended important behavior should sometimes be reduced. In the present studies, the strain rate influence to the material behaviors has been confirmed to be quite negligible, so that it was ignored and not referred in parameter evaluation. No comparison between the experimental and the simulated cyclic curves with different strain rate were carried out here. The strain rate dependency gives the influence mainly to the parameters K and n. In the present studies, a relaxation test was employed to help determination of these parameters.

8.3 Property of the Neural Identification Method

8.3.1 Advantages of the Method

The neural identification procedure has the following three main advantageous characteristics :

1) The learning system is independent of the employed model.
2) Using the learned tool requires an operator to have neither special skill nor experience on a neural network and the employed constitutive equation.
3) As many reference experimental data as available can be taken into reference data.

For the first advantage, the tool is more convenient if which of the models available suits to the target phenomenon has not yet been determined. The learning system should not be changed depending on the models, because the basic prediction theory of the neural network is simple calculation of the output values from the input values with the tuned up internal neural parameters, weights and off-set values, which are learned to map the correct relationship between the input and the output values (training patterns). When any different model is taken into consideration, only the relationship to be learned should be re-prepared. Furthermore, since all the other parts of the training procedure besides the relationship are the same in all cases, the comparison of the results by different viscoplastic models can be done with the same groups of reference experimental data.

For the second advantage, this procedure with a neural network has been developed to be used without experience or skill on the neural network or viscoplastic constitutive equations. After the training procedure, neither special experience nor skill is needed for an operator, which makes any operator be able to use the tool and obtain the parameters included in viscoplastic constitutive equations. Parameter identification in the neural method is essentially the prediction without external consideration (the black box prediction).

For the third advantage, all the input data are referred equally, and the evaluation results are positioned just at the center of the data field. The method is the more reliable with the more reference data.

8.3.2 Disadvantages of the Method

The learning relationship should be prepared for each model or each condition if it is needed, for an example, the temperature condition in the present studies. Chaboche's model has the temperature dependent parameters. For each temperature case, each behavior simulation with a different

Young's modulus draws the different behavior curves. (The simulation described in Chapter 3 was carried out with Young's modulus corresponding to T = 200℃.) The neural method needs a lot of training patterns.

Without some information of evaluation results by means of a numerical identification method, it is more difficult to choose the learning field (number of the training patterns). This is coming from such a fact that a neural network can only interpolate, i.e., the results must be found within the learned field. If the actual result is outside the learned field, a neural network can not evaluate the output value at all. It is normally very difficult to evaluate accurate output values with a smaller learning field, and generally a larger learning field is needed. In the present studies, if the results to be estimated were not successfully obtained by means of the numerical identification, the learning field of the neural network with seven parameters had to be considerably large, for an example, over 10000 training patterns. The related research results are as follows :

1) If learning field (training patterns) is chosen cross-linked as shown in Figure 8.3.2.1, the prediction accuracy field will be as shown in Figure 8.3.2.2.
2) If learning field (training patterns) is chosen matrix-shaped as shown in Figure 8.3.2.3, the prediction accuracy field will be as shown in Figure 8.3.2.4.

In the present studies, the most serious problem is that the employed Chaboche's theory is not completely correct. (Every viscoplastic theory proposed previously is not completely correct as well.) Therefore, the actual relationship between the parameter set and the experimental behaviors must be slightly different from the simulated relationship, even if the parameter set or the behaviors of these simulated and the actual cases are the same. The evaluation results become worse if the experimental behaviors (input data whose corresponding parameter set is unknown) deviate from the employed model.

8.3.3 Further Comments on the Method

The number of input data is important at the point of how precisely each behavior should be referred and how many data points should be needed to evaluate the parameter set accurately. The determination is deeply related with the primitive idea of the application (see the next sub-section). Here, the number of the input data from the experimental data field suggests the degree of its importance how to be referred. Before the learning, enough research on the employed model and the application target phenomena should be surveyed.

How to choose the learning field is also of considerable importance for such a point that a neural network can hardly predict a target outside of the learning field. Before the evaluation by this tool, some preliminary research on the rough prediction of the target field is needed, for which the previously mentioned numerical method is one of the best tools. However, it is still possible that the neural method is used without any help just for the comparison of roughly predicted results corresponding to different models or materials. In this case, a certain detailed research, for an example, parameter evaluation by the numerical method, should follow after rough evaluation. The

neural identification method may mainly be expected to be applied to the discussions on which model is the best applicable to an attended problem without any information on it.

The evaluation capability by this tool is summarized as follows : On a personal computer with a neuro-hard board (which has been developed by CRC), input data number (input unit number) of over 50 and the training patterns of over 89 enabled to evaluate the parameter set by discrepancy of 7 to 12 %. The necessary calculation time was about 32 hours. The reliability of each evaluation result was somewhat worse than that by a numerical method, while the curve fitting was done under equal reliability for all the referred experimental behaviors. This tool may be recommended to be used for comparison of the evaluation results with respect to different models or conditions, and for fitting to various different behaviors as a whole.

8.4 Expectations for General Application of Parameter Identification with a Viscoplastic Constitutive Equation

8.4.1 Principle Idea of the Application

Essentially, the development of the parameter identification method for application of a viscoplastic model to the lifetime prediction is for the ill-structured material. The complete behavior of the ill-structured material can never be explained by single theory, and a certain approximation using a viscoplastic constitutive equation is needed. The newly developed two identification methods are the tools which can evaluate the most convenient parameter set for the real behavior. The parameter set can never be identified correctly, and should never be identified correctly. The most important idea is that the approximation with the viscoplastic model should be as accurate to draw the attended behaviors as it can.

8.4.2 Consideration on Evaluation Error

In the present studies, two different kinds of evaluation errors exist. At first, such an evaluation error exists as follows :

1) The pure fitting error of the simulated behavior curves with the evaluated parameter values to the experimental curves based on a least square method during each evaluation procedure in the both identification method.
2) The prediction accuracy depending on the training patterns number, the input units number, the hidden units number and the training patterns field in the numerical identification method.

The fitting errors which are considered as the problem of the identification method are handled in the numerical method, or re-calculated after tuning the neural parameters. The final error may be the magnitude of difference on the behavior curves between the simulated with the evaluated parameter values and the experiments. Here, the finally aimed magnitude of the final error should be determined in the future, while the discussions on it should be done at the beginning of the research works as the primitive idea of application of a viscoplastic model to the real phenomenon.

The accuracy on the simulated material behaviors with the evaluated parameter set affects the lifetime prediction. Since every viscoplastic model is not correct, the calculated lifetime prediction must not be completely correct with any parameter set. Therefore, the lifetime prediction should be available with consideration of the danger ratio. Here, the accuracy does not have to increase unlimitedly but a few % of error may be allocated.

8.4.3 Extension to Multiaxial Cases

Parameters included in the most viscoplastic theories can be determined from uniaxial experiments. However, determination of the parameters from multiaxial tests is necessary in the following two cases :

1) The model is developed for anisotropic materials.
2) The model is developed for initially isotropic materials but is capable of explaining additional hardening under non-proportional loading.

It is easy for a neural method to be applied to the multiaxial forms if the training procedure can be furnished suitably, while the training procedure will become more complicated to simulate the parameter influence to the reference behaviors. On the other hand, it is very difficult for a numerical method to be established and to modify the parameter values in detail comparing the simulated behaviors with the experimental behaviors. This establishment needs detailed research on the multiaxial forms. The more possibility to determine the multiaxial parameters by a neural met work may exist, because the numerical identification can not be expected to give accurate evaluation results any further. The results by a neural method may have more then 20 to 30 % discrepancy, which can be regarded as not being negligible at this moment.

Furthermore, experiments which should be referred to the parameter identification become more difficult to be carried out under the multiaxial condition to obtain the available data. It is rather important to approximate the real phenomena to be in the simplest loading field, and to discuss the application of the uniaxial model to the multiaxial field.

8.4.4 Application to Any Model

The possibilities of generally applying these two identification methods to other models have been discussed in the previous sub-sections. Not only viscoplastic but also non-viscoplastic models can theoretically be applied, while viscoplastic models are needed to explain the material behavior better for the lifetime prediction. The discussions on the characteristics of each viscoplastic theory have currently been in progress and new other theories are presently coming out. The important attention is that how to explain the material behavior with the constitutive equations and how to determine the parameters included in the constitutive equations are essentially different problems. The viscoplastic model which is nearly complete is not available if the parameters can be hardly evaluated based on the experimental data. Not the correct model whose parameter set can be hardly determined, but the more convenient model, which is almost correct and whose parameter set can be well evaluated, is expected actually.

To determine which is the best model to the attended problem is of importance. Some information about it may be obtained from theoretical research works, while some different models should sometimes be employed to the same phenomenon to compare their characteristics. Finally, experiments are expected to confirm all the calculated results (parameter evaluation, lifetime prediction and so on). Related with the present studies, the experiments on the geometry given in Figure 7.2.1.1 are performed with the European Fusion Program, which will confirm the lifetime prediction results described in Chapter 7.

Other possibility to predict the material behaviors by a neural network may exist. If a lot of experimental behaviors which have been obtained can be learned to a neural network not with the corresponding parameter set but with the corresponding test conditions and the corresponding material, the neural network will predict a certain behavior directly. Such behavior prediction without consideration of constitutive equations may be also useful in the future.

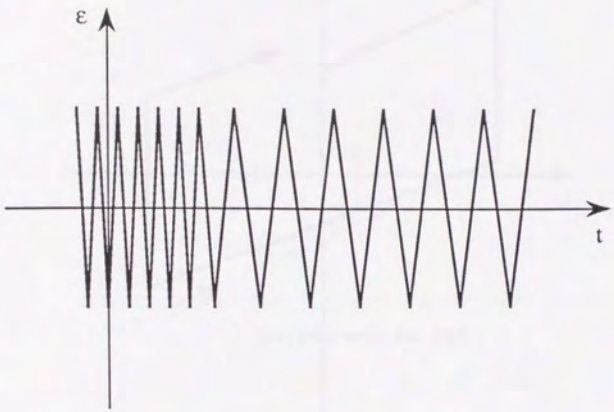

Figure 8.1.1.1 : An example of the strain rate shift

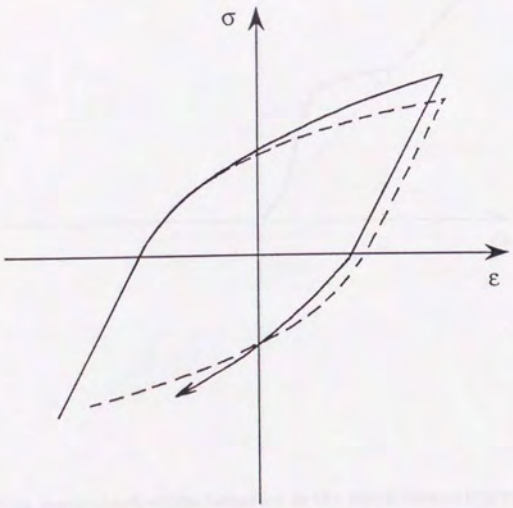

Figure 8.1.1.2 : Hysteresis loop shift corresponding to the strain rate shift

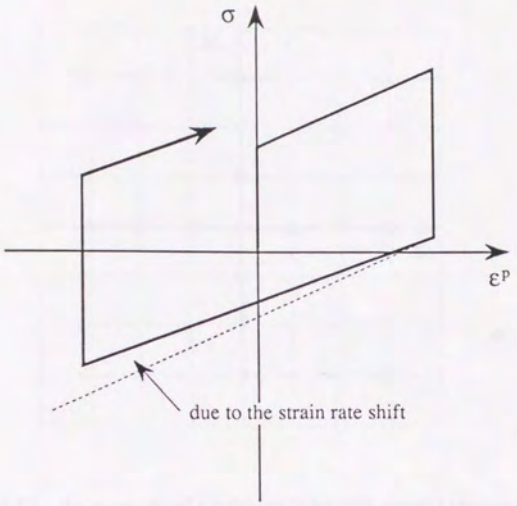

Figure 8.1.1.3 : An example of the proposed non-linear relationship between stress and strain rate

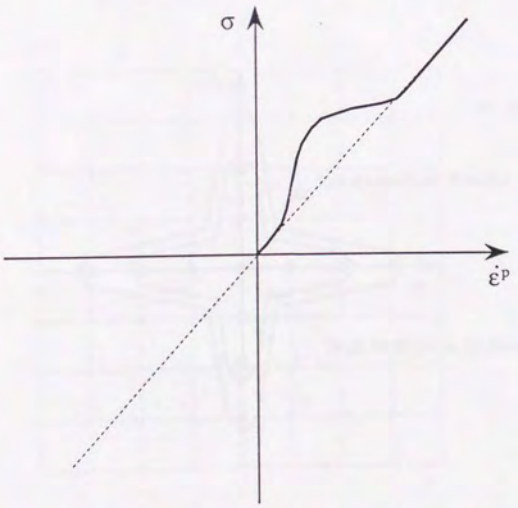

Figure 8.1.1.4 : Non linear-back stress behavior in the stress-inelastic strain rate relatiohship

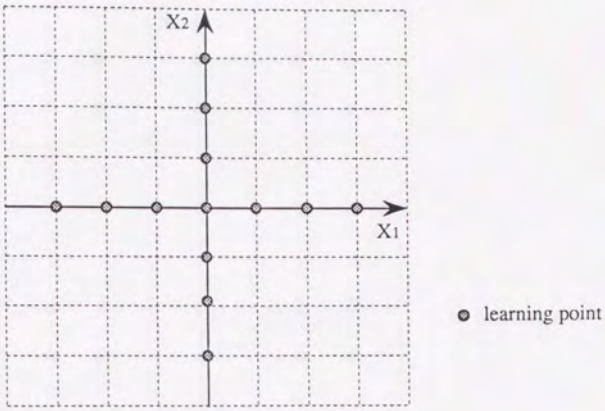

Figure 8.3.2.1 : An example of a learning field with crossly chosen patterns (two-dimensional)

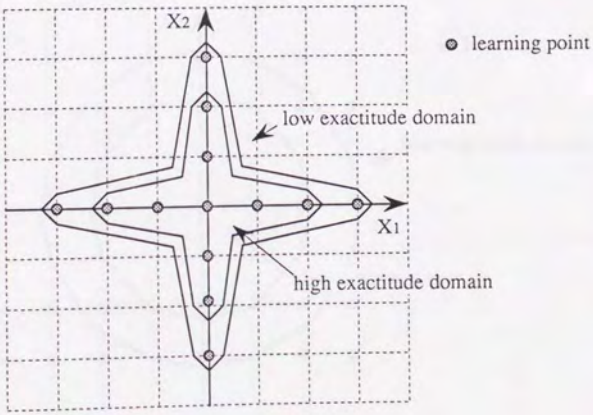

Figure 8.3.2.2 : The accuracy distribution of the evaluation results for a learning field with crossly chosen patterns (two-dimensional)

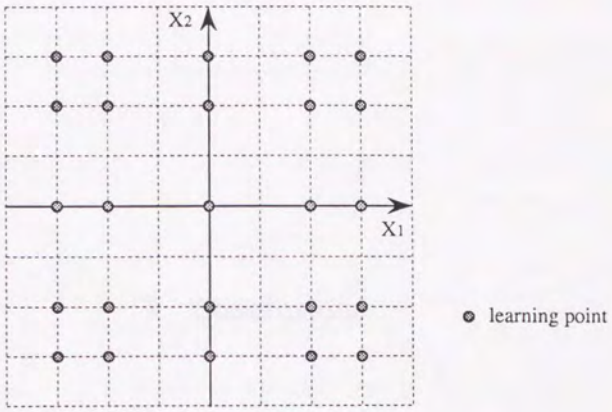

Figure 8.3.2.3 : An example of a learning field with matrixwise chosen patterns
(two-dimensional)

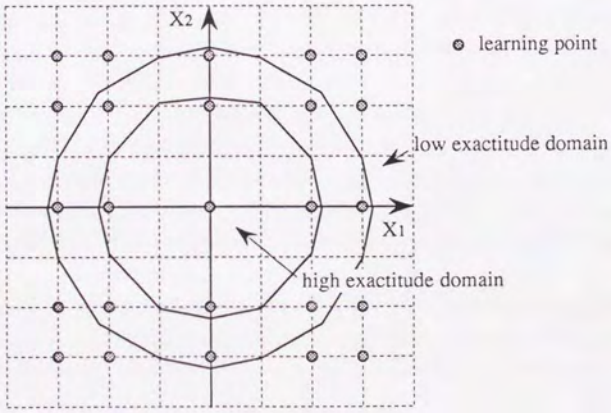

Figure 8.3.2.4 : The accuracy distribution of the evaluation results
for a learning field with matrixwise chosen patterns
(two-dimensional)

9 Conclusions

For the purpose of predicting the lifetime of the first wall of a fusion reactor during the normal operation which exceeds the elastic domain, the uniaxial forms of Chaboche's viscoplastic constitutive equations were considered to be applied to non-linear thermo-inelastic FE analyses. The parameters included in Chaboche's constitutive equations were determined by a new evaluation method based on experimental data of cyclic tests and succeeding relaxation tests. In the following, the present studies are summarized with their conclusions.

1) The experimental tests simulating the thermo-mechanical cyclic loading under the first wall condition were performed on the test specimen made by type SS 316L SPH stainless steel.

The tests consisted of cyclic tests and succeeding relaxation tests. The temperature during the experiments were fixed in the range of interest, 200℃ and 400℃. The stress strain histories obtained from these experiments were recorded numerically onto floppy disks.

2) The parameter identification methods were developed along the following two different approaches. The principles of these methods can also be applied to evaluate the parameter set included in other viscoplastic constitutive equations.

One is the method with a numerical computation. The method can numerically treat a great amount of experimental data, which contribute toward more accurate evaluation and detailed confirmation related to the physical significances of the parameters. The evaluated parameter sets for two cases of temperature T = 200℃ and 400℃ simulated the cyclic and relaxation curves in quite satisfactory agreement with experimental curves. This suggests that this newly developed procedure employing numerical computation based on experimental stress-strain data of cyclic tests with sufficient cycles and succeeding relaxation tests can determine a suitable parameter set for Chaboche's viscoplastic constitutive equations with much better accuracy in comparison with those in the previous studies.

The other was the method with a neural network. The method can predict the relationship between the stress strain histories and the parameter sets after a training procedure. Special skill or knowledge for the employed viscoplastic model or the neural network is not necessary after a training procedure. With this method, various material behaviors can be referred simultaneously to evaluate the parameters set which is related to all these behaviors. The evaluated parameter sets for two cases of temperature T = 200℃ and 400℃ simulated the experimentally obtained tensile, cyclic, hardening and relaxation curves with good agreement, which suggests that this newly developed procedure employing a neural network based on experimental stress-strain data of cyclic tests with sufficient cycles and succeeding relaxation tests can also search a suitable parameter set for Chaboche's viscoplastic constitutive equations.

3) Chaboche's constitutive equations were confirmed their applicability to the behavior of the first wall material under the operation condition with a uniaxial condition.

For the lifetime prediction of the first wall, the curve fitting on the cyclic behavior of type SS 316L SPH stainless steel under the stationary temperature conditions of T = 200℃ and 400℃ was

performed with Chaboche's model. With these two different methods, the parameter sets included in the uniaxial stationary temperature form of Chaboche's viscoplastic constitutive equations can be well evaluated. The simulated cyclic behavior showed good agreement with those from experiments, and it became clear that the Chaboche's model can simulate the cyclic behavior of the first wall material within the temperature range of interest T = 200℃ to 400℃.

4) The lifetime prediction of the first wall with different material models suggested that viscoplastic model is necessary.

The Chaboche's model with the parameter sets evaluated by the numerical method was implemented in the ABAQUS FE-code and applied to calculate the cyclic stress-strain field of fusion machines. Then lifetime prediction by different models were performed. The lifetime prediction by the Chaboche's constitutive equations for one of the first wall candidate materials SS 316L SPH showed the most sever result as to the crack initiating cycles. The prediction results should be further confirmed by experiments on the first wall.

References

Chapter 1

1.1 G. Vieider, W. Daenner and B. Haverkamp : Design Concepts for NET First Wall and Blankets. Fusion Technology, Vol. 2, (1984). Proceedings of the 13 th SOFT, p.1363, (1984).

1.2 INTOR Phase 1, International atomic energy agancy, Vienne, (1982).

1.3 T. Fett and D. Munz : Stress and Lifetime Calculations for First Wall and Blanket Structural Components, Part I, Crack Propagation in tubes. KfK 3875, (1985).

1.4 E. Diegele, T. Fett, D. Munz and H. Stamm : Stress and Lifetime Calculations for First Wall and Blanket Structural Components, Part II, Crack Propagation in the NET First Wall. KfK 4210, (1987).

1.5 K. P. Walker : Research and Development Program for Nonlinear Structural Modeling with Advanced Time-Temperature Dependent Constitutive Relationships. Final Report, NASA CR-165 533, (1981).

1.6 J. Eftis and D. L. Jones : Evaluation and Development of Constitutive Relationships for Inelastic Behavior. Final Report, Air Force Office of Scientific Research, Washington, D. C., (1983).

1.7 J. Eftis, J. S. Abdel-Kader and D. L. Jones : Comparisons Between the Modified Chaboche and Boder-Partom Viscoplastic Constitutive Theories at High Temperature. Int. J. Plasticity, Vol. 5, p.1, (1989).

1.8 S. S. Chiu, J. Eftis and D. L. Jones : Trans. ASME, Vol. 112, p.188, (1990).

1.9 J. L. Chaboche and G. Rousselier : On the Plastic and Viscoplastic Equations, Part I = Rules Developed with Internal Variable Concept, J. Pressure Vessel Tech., Vol. 105, p.153, (1983).

1.10 J. L. Chaboche and G. Rousselier : On the Plastic and Viscoplastic Equations, Part II = Application of Internal Variable Concepts to the 316 Stainless Steel, J. Pressure Vessel Tech., Vol. 105, p.159, (1983).

1.11 G. Cailletaud and J. L. Chaboche : Macroscopic Description of the Microstructural Changes Induced by Varying Temperature, Example of in 100 Cyclic Behaviour, Communication presentation " Third International Conference on Mechanical Behavior of Materials" ICM-3, Cambridge, Aug. 20-24, (1979).

Chapter 2

2.1 M. A. Leontorich (Edited) : Review of Plasma Physics Vol. 5, p.349, (1970).

2.2 J. Darvas : Proc. of 11th Int. Conf. on Effects of Radiation on Materials, ASTM STP 782, (ASTM, Philadelphia, 1982), p.1140.

2.3 (in Japanese) G. Yagawa : The Fusion Studies, Vol. 56, p.248, (1986).

2.4 G. Vieider and A. Cardella : Estimated thermal fatigue limits for the first wall of NET. Proc. of the IAEA Technical Commitee Meeting on Lifetime Predictions for the First Wall and Branket

Structure of Fusion Reactors, 5-7, p.149, Karlsruhe, Nov., (1985).

2.5 (in Japanese) JAERI, Development Situation of the Fusion Studies, (1985).

2.6 (in Japanese) JAERI, Report on Discussions of the Fusion Design, (1988).

2.7 R. J. Leclaire and J. E. Meyer : J. Fusion Energy, Vol. 42 No. 5, p.353, (1985).

2.8 P. Blanchard, P. May and H. Scheurer : Fusion Tech., Vol. 2, p.749, (1983).

2.9 K. P. Walker : Research and Development Program for Nonlinear Structural Modeling with Advanced Time-Temperature Dependent Constitutive Relationships, Final Report NASA CR-165 533, (1981).

2.10 K. P. Walker : Representation of Hastelloy-X Behavior at Elevated Temperature with a Functional Theory of Viscoplasticity. Presented at ASME/PVP Century 2 Emerging Technology Conference, San Francisco, California, Aug., (1980).

2.11 U. S. Lindholm et al. : Constitutive Modeling for Isotropic Materials. First Annual Report NASA CR-174 718, (1984).

2.12 G. Hartmann : Vergleich des einachsigen Verhaltens dreier inelastischer Werkstoffmodelle mit internen Zustandsvariablen durch numerische Experimente. Dissertation, TH Darmstadt, (1988).

2.13 K. P. Walker : Constitutive Modeling of Engine Materials. Final Report FR-17911 to AMFL Contract F33615-81-C5040, (1983).

2.14 E. Kermpl : The Role of Servocontrolled Testing in the Development of the Theory of Viscoplasticity Based on Total Strain and Overstress. Presented as the ASTM Symposium on Mechanical Testing for Deformation Model Development, Bal Harbour, Florida, Nov. 12-13, (1980).

2.15 E. P. Cernocky and E. Krempl : A Nonlinear Uniaxial Integral Constitutive Equation Incorporating Rate Effects, Creep and Relaxation. Int. J. of Nonlinear Mechanics, Vol.14, p.183, (1979).

2.16 J. Schwertel : Internal Report of KfK, IMF-4, 13-02-03P26A, p.53, May, (1990).

2.17 J. L. Chaboche : Viscoplastic Constitutive Equations for the Description of Cyclic and Anisotropic Behavior of Metals. Bulletin de L'Academis des Sciences, Serie des Sciences Techniques, Vol.15, No.1, p.33, (1977).

2.18 J. L. Chaboche : Thermodynamic and Phenomenological Description of Cyclic Viscoplasticity with Damage. Translation of Publication No.1978-3 of the Office National d'Etudes et de Researches Aerospatiales, France, by the European Space Agency Technical Translation Service, Publication Number ESA-TT-548, May, (1979).

2.19 A. K. Miller : An Inelastic Constitutive Model for Monotonic, Cyclic and Creep Deformation, Part I = Equations Development and Analytical Procedures, Part II = Application to Type 304 Stainless Steel. ASME, J. Eng. Mat. & Tech., Vol.98, p.97, (1976).

2.20 A. K. Miller : The MOTMOD Equations. In: Unified Constitutive Equations for Creep and Plasticity ed. by A. K. Miller, Elsevier Appl. Science Publ., (1987).

2.21 C. G. Schmidt and A. K. Miller : A Unified Phenomenological Model for Non-Elastic Deformation of Type 316 Stainless Steel. Part I = Development of the Model and Calculation of the Material Constants, Part II = Fitting and Predictive Capabilities. Res. Mechanica, Vol.3, p.109 and p.175, (1981).

2.22 O. D. Sherby and C. M. Young : Some Factors Influencing the Strain Rate-Temperature Dependence of the Flow Stress in Polycrystalline Solids. In: Symposium on Rate Processes in Plastic Deformation of Materials, Amer. Soc. for Metals, p.497, (1975).

2.23 D. C. Stouffer and S. R. Bodner : A Constitutive Model for the Deformation Induced Anisotropic Plastic Flow of Metals. Int. J. Eng. Sci., Vol. 17, p.757, (1979).
2.24 R. W. young : A Note on the Stouffer-Bodner Constitutive Model for Anisotropic Plastic Flow. Lett. Appl. Eng. Sci., Vol. 18, p.1091, (1978).
2.25 S. R. Bodner and Y. Partom : Constitutive Equations for Elastic-Viscoplastic Strain Hardening Materials. ASME, J. of Applied Mechanics, Vol. 42, p.385, (1975).
2.26 E. W. Hart : Constitutive Relations for the Nonelastic Deformation of Metals. ASME, J. of Eng. Mat. & Tech., Vol.98, p.193, (1976).
2.27 T. J. Delph : A Comparative Study of Two State-Variable Constitutive Theories. ASME, J. of Eng. Mat. & Tech., Vol.102, p.327, (1980).
2.28 D. N. Robinson : A Unified Creep-Plasticity Model for Structural Metals at High Temperature. Eng. Tech. Division, Contract No. W-7405-eng-26, Oct., (1978).
2.29 D. N. Robinson and P. A. Bartolotta : Viscoplastic Constitutive Relationship with Dependence on Thermomechanical History. NASA Contractor Report 174836, March, (1985).
2.30 K. Hornberger : Internal Report of KfK, IMF-4, 13-02-03P26A, pp.3-52, May, (1990).

Chapter 4

4.1 S. Karl : Deformationsverkalfen des Stahles 1.4909 unter verrieren den Lastgeschichten, Studienar bei 7 am IZSM, Universität Karlsruhe, (1991).
4.2 G. L. Tjoa, et al. : Netherlands Energy Research Foundation, Report ECN-135, July, (1983).
4.3 Betriebsanleitung, Schenck. PEZ 8249, Erwieterung der POZ 863, Hydropuls-Prüfmaschine 63kN.
4.4 J. Schwertel, B. Schinke, U. Spermann and D. Munz : 3rd Int. Conf. on Constitutive Laws for Engineering Materials and Workshop, Tucson, Arizona, Feb., (1991).

Chapter 7

7.1 Hibbit, Karlson, Sorensen, Inc. ABAQUS User's Manual. Providence, RI, (1988).
7.2 Nuclear Standard NE. F. 9-5T, Guidelines and Procedures for Design of Classical Elevated Temperature Nuclear System Components, U. S. Department of Energy, Nuclear Energy Programs, March, (1981).
7.3 Afcen RCC-MR, Règles de Conception et de Construction des Matériaux Mécaniques des Ilots Nucléaires RNR, Annexe Technique A3, (1985).

Appendices

A1.1 Basic Theory

It is very complicated to describe correctly the viscoplastic, stress-strain field in metallic material, while the following theory has been employed for the primary consideration of the field. In this section, the primary relation between stress and strain with the separation of inelastic behavior from elastic behavior is explained.

The behavior can be separated into two components, the deviatoric (or distortional or shear) behavior and the bulk (or volumetric or spherical) behavior. The behaviors of material under loading condition are generally discussed with the following equations on stress σ_{ij} and strain ε_{ij} :

$$\varepsilon_{ij} = e_{ij} + \frac{\varepsilon_{kk}}{3}\delta_{ij} \qquad (A1.1.1)$$

$$\sigma_{ij} = s_{ij} + \frac{\sigma_{kk}}{3}\delta_{ij} \qquad (A1.1.2)$$

where δ_{ij} is the Kronecker delta. In each equation, the first term and the second term of the right side mean the deviatoric behavior and the bulk behavior, respectively. Some authors define the second term without dividing by 3.

The bulk behavior is to say the elastic volume change. On the bulk part, bulk stress σ_{kk} and bulk strain ε_{kk} should be correlated by the following relation :

$$\varepsilon_{ij} = J\,\sigma_{ij} \qquad (A1.1.3)$$

where J is the elastic bulk modulus which is a material constant.

While, the deviatoric behavior is to say the configuration change, which is caused by both elastic and inelastic mechanisms. Therefore, on the deviatoric part, deviatoric strain e_{ij} should be divided into two separate parts as follows :

$$e_{ij} = e^{e}_{ij} + e^{p}_{ij} \qquad (A1.1.4)$$

where the superscripts, e and p, denote the elastic part and the plastic part, respectively. The following relations between deviatoric stress s_{ij} and deviatoric strain e^{e}_{ij} and e^{p}_{ij} may be written.

$$e^{e}_{ij} = \frac{s_{ij}}{2G} \qquad (A1.1.5)$$

$$\dot{e}^{p}_{ij} = F(\xi) \qquad (A1.1.6)$$

where G and F are the elastic shear modulus and a certain function of deviatoric stress field ξ, respectively, which depend on the material property.

To obtain easier expressions, bulk strain and elastic deviatoric strain may be treated together as elastic strain ε^{e}_{ij}. On the other hand, plastic deviatoric strain is denoted by ε^{p}_{ij}. Then, the following formula is followed :

$$\varepsilon_{ij} = \varepsilon^{e}_{ij} + \varepsilon^{p}_{ij} \qquad (A1.1.7)$$

where

$$\varepsilon^{e}_{ij} = \frac{\varepsilon_{kk}}{3}\delta_{ij} + e^{e}_{ij} \qquad (A1.1.7a)$$

$$\varepsilon^{p}_{ij} = e^{p}_{ij} \qquad (A1.1.7b)$$

Here, ε_{ij} can be called the total strain. Its differential form should be as follows :

$$\dot{\varepsilon}_{ij} = \dot{\varepsilon}^{e}_{ij} + \dot{\varepsilon}^{p}_{ij} \qquad (A1.1.8)$$

As mentioned later, relation A1.1.6 is often described by a differential form, for plastic strain depends on strain rate.

In the following discussion, any effect of temperature to the behavior is almost ignored, so that creep behavior and plastic behavior would be only the inelastic parts which are to be discussed. Since creep behavior has very similar characteristics to plastic behavior, it may be included into the plastic part of the behavior. Therefore, plastic strain ε^{p}_{ij} means creep and plastic strain as inelastic strain.

A1.2 General Elastic Relation of Stress and Strain

In this section, the relation between elastic strain, which is defined in relation A1.1.7a, and stress is discussed. The elastic deformation is completely recovered after unloading on the theory.

The general relation between stress σ_{ij} and elastic strain ε^{e}_{ij} is led from relations A1.1.3, A1.1.5 and A1.1.7a as follows :

$$\varepsilon_{ij} = J\frac{\sigma_{kk}}{3}\delta_{ij} + \frac{s_{ij}}{2G} \qquad (A1.2.1)$$

$$= \left(J - \frac{1}{2G}\right)\frac{\sigma_{kk}}{3}\delta_{ij} + \frac{1}{2G}\sigma_{ij}$$

The relation A1.2.1 in a three-dimensional space (x1, x2, x3) can be expressed in a matrix form of the order nine (three times three dimensions) as follows :

$$\varepsilon^e_{ij} = \begin{pmatrix} \varepsilon^e_{11} \\ \varepsilon^e_{12} \\ \varepsilon^e_{13} \\ \varepsilon^e_{21} \\ \varepsilon^e_{22} \\ \varepsilon^e_{23} \\ \varepsilon^e_{31} \\ \varepsilon^e_{32} \\ \varepsilon^e_{33} \end{pmatrix} = \begin{pmatrix} m_a & 0 & 0 & 0 & m_b & 0 & 0 & 0 & m_b \\ 0 & \frac{1}{2G} & 0 & 0 & 0 & 0 & 0 & 0 & 0 \\ 0 & 0 & \frac{1}{2G} & 0 & 0 & 0 & 0 & 0 & 0 \\ 0 & 0 & 0 & \frac{1}{2G} & 0 & 0 & 0 & 0 & 0 \\ m_b & 0 & 0 & 0 & m_a & 0 & 0 & 0 & m_b \\ 0 & 0 & 0 & 0 & 0 & \frac{1}{2G} & 0 & 0 & 0 \\ 0 & 0 & 0 & 0 & 0 & 0 & \frac{1}{2G} & 0 & 0 \\ 0 & 0 & 0 & 0 & 0 & 0 & 0 & \frac{1}{2G} & 0 \\ m_b & 0 & 0 & 0 & m_b & 0 & 0 & 0 & m_a \end{pmatrix} \begin{pmatrix} \sigma^e_{11} \\ \sigma^e_{12} \\ \sigma^e_{13} \\ \sigma^e_{21} \\ \sigma^e_{22} \\ \sigma^e_{23} \\ \sigma^e_{31} \\ \sigma^e_{32} \\ \sigma^e_{33} \end{pmatrix} = [\, M \,]\, \sigma_{ij} \qquad (A1.2.1')$$

where

$$m_a = \frac{J}{3} + \frac{1}{3} \qquad (A1.2.2)$$

and

$$m_b = \frac{J}{3} - \frac{1}{6G} \qquad (A1.2.3)$$

On the other hand, under uniaxial loading, Fuck's law suggests such a stress-strain relationship independently as follows :

$$\varepsilon^e_{11} = \frac{1}{E}\sigma_{11} \qquad (A1.2.4a)$$

$$\varepsilon^e_{22} = \varepsilon^e_{33} = -\frac{\nu}{E}\sigma_{11} \qquad (A1.2.4b)$$

where subscript 1 means the loading direction and no deviatoric strain occurs in this case. The elastic modulus (or Young's modulus) and Poisson's ratio have been denoted by E and ν, respectively.

Since relation A1.2.1 with uniaxial stress ($\sigma_{ij} = 0$, except for the component σ_{11}) is equivalent to relations A1.2.4a and A1.2.4b, the following relations among moduli J, G, E and ν should stand :

$$E = 2G(1+\nu) \qquad (A1.2.5a)$$

$$J = \frac{1-2\nu}{E} \qquad (A1.2.5b)$$

Hence, relation A1.2.1 can also be expressed as follows :

$$\varepsilon^e_{ij} = \frac{1+\nu}{E}\sigma_{ij} - \frac{\nu}{E}\sigma_{kk}\delta_{ij} \qquad (A1.2.6)$$

whose differential form is led as follows :

$$\dot{\varepsilon}^e_{ij} = \frac{1+\nu}{E}\dot{\sigma}_{ij} - \frac{\nu}{E}\dot{\sigma}_{kk}\delta_{ij} \qquad (A1.2.6')$$

Normally, these relations A1.2.6 and A1.2.6' are used to discuss stress-strain field. It has been mentioned that elastic strain is independent of strain rate (rate-independent).

A1.3 Inelastic Relation of Stress and Strain

In this section, the basic concept on the relation between stress and inelastic strain is discussed. The deformation which can not be completely recovered after unloading may be explained with the relation between stress (or deviatoric stress) and inelastic strain rate, since inelastic strain depends on strain rate (rate-dependent).

In relation A1.1.6, inelastic field ξ is normally considered to be $(\sigma_{ij} - Y_{ij})$ or $(s_{ij} - Y_{ij})$, where Y_{ij} is back (or equilibrium or rest) stress, which is a state variable for a kinematic hardening modulus. Here, stress σ_{ij} (or deviatoric stress s_{ij}) and back stress Y_{ij} may be called external and internal stress, respectively. The reason why $F(\xi)$ is considered not to be a function of σ_{ij} or Y_{ij} separately but to be that of $(\sigma_{ij} - Y_{ij})$ is that it is very complicated to treat the former type of a function mathematically. While, a tensor function $F(\xi) = F_{ij}(\xi)$ is generally expressed as follows :

$$F(\xi) = F(\sigma_{ij} - Y_{ij}) = F_0[A_0(\sigma_{ij} - Y_{ij})]\delta_{ij} + F_1[A_1(\sigma_{ij} - Y_{ij})](\sigma_{ij} - Y_{ij}) + F_2[A_2(\sigma_{ij} - Y_{ij})](\sigma_{ik} - Y_{ik})(\sigma_{kj} - Y_{kj}) + \cdots\cdots \quad (A1.3.1)$$

where each component, δ_{ij}, $(\sigma_{ij} - Y_{ij})$ or $(\sigma_{ik} - Y_{ik})(\sigma_{kj} - Y_{kj})$ appeared in the right side of relation A1.3.1 means tensor of $F(\xi)$. Now a day, the first term of the right side of relation A1.3.1 is regarded as zero, and all terms beyond the third term are ignored to make the expression easier as follows :

$$F(\xi) = F_1[A_1(\sigma_{ij} - Y_{ij})](\sigma_{ij} - Y_{ij}) \quad (A1.3.2)$$

Based on the above mentioned primary expression, the special form can be led under such conditions as :

1. isotropic assumption on the material ($\sigma_{ij} = \sigma_{ji}$, and $\varepsilon_{ij} = \varepsilon_{ji}$)
2. incompressive inelastic response of the material ($\varepsilon^p_{kk} = 0$)

The special form of the relation for inelastic strain rate $\dot{\varepsilon}^p_{ij}$ is allowed to be written as follows :

$$\dot{\varepsilon}^p_{ij} = f\left(\frac{\sigma_{ij} - Y_{ij}}{K}, R\right) \times (\sigma_{ij} - Y_{ij}) \quad (A1.3.3)$$

where f is a certain tensor function and $f \times f^{-1} = E$. Here, Y_{ij} and R are state variables called back stress and isotropic hardening, respectively. K and R are isotropic hardening material constants.

Mainly, material characteristics are explained in the inelastic part of its behavior.

Three following evolution laws in Y, R and K can be written to incorporate strain hardening and cyclic hardening into the viscoplastic theories :

$$\dot{Y}_{ij} = f_{Y1}\dot{\varepsilon}^{p}_{ij}\,\delta_{ij} - f_{Y2}Y_{ij}|\dot{\varepsilon}^{p}_{ij}| - f_{Y3}|Y_{ij}| \qquad \text{(A1.3.4a)}$$

$$\dot{R} = f_{R1}\dot{\varepsilon}^{p}_{ij} - f_{R2}Y|\dot{\varepsilon}^{p}_{ij}| - f_{R3}|R| \qquad \text{(A1.3.4b)}$$

$$\dot{K} = f_{K1}\dot{\varepsilon}^{p}_{ij} - f_{K2}Y|\dot{\varepsilon}^{p}_{ij}| - f_{K3}|K| \qquad \text{(A1.3.4c)}$$

where f_x's (where x = Y_1, Y_2, Y_3, R_1, R_2, R_3, K_1, K_2 or K_3) are certain scalar functions of Y_{ij}, R or K. The first, the second and the third terms of each expression express hardening, dynamic recovery and static thermal recovery, respectively. Expressions A1.3.4a and A1.3.4b involve physical meanings. First, as they increase from the initial values of Y_{ij} and R ($R_0 = 0$), the recovery terms become dominant. That suggests their saturation. Second, when stress is fixed and $\varepsilon^{p}_{ij} = \varepsilon_{ij}$, large strain rate causes increasing back stress and decreasing strain rate. That explains the primary creep behavior with transient period of high strain rate to be a stable state. Third, if strain rate decreases down to zero due to stress disappearance, Y_{ij} (with $\dot{Y} = -f_{Y3}|Y_{ij}|$) and R (with $\dot{R} = -f_{R3}|R|$) also decrease. That suggests inelastic strain recovery. These facts are observed on many metallic materials, while these evolution laws can be considered very suitable for these material.

A1.4 Relation between Elastic and Inelastic Behaviors

In this section, elastic and inelastic behaviors are visually explained. Here, it is actually impossible to divide material strain behavior into two parts, elastic and inelastic parts, completely.

Based on expression A1.1.4, stress σ, elastic strain ε^e, inelastic strain ε^p, total strain ε, are determined under a uniaxial cyclic stress loading condition as shown in Figure A1.4.1, which is drawn theoretically. At points A, B and C, ε^p is clearly greater than zero, equal to zero and less than zero, respectively, because of expression A1.2.1, and during the elastic domain, it is clearly constant.

The following derivatives of σ are sometimes discussed :

$$\frac{d\sigma}{d\varepsilon}\ ,\ \frac{d\sigma}{d\varepsilon^e}\ ,\ \frac{d\sigma}{d\varepsilon^p}$$

As shown in Figure A1.4.2, these values are originally different from one another. The following approximate relation A1.4.1a or A1.4.1b is, however, allowed only in the elastic domain or in the saturation inelastic domain :

$$\frac{d\sigma}{d\varepsilon} = \frac{d\sigma}{d\varepsilon^e} \qquad \text{for elastic domain} \qquad (A1.4.1a)$$

$$\frac{d\sigma}{d\varepsilon} = \frac{d\sigma}{d\varepsilon^p} \qquad \text{for inelastic domain} \qquad (A1.4.1b)$$

where relation A1.4.1b is not completely correct and the following correlation actually stands theoretically :

$$\left[1 - \frac{d\sigma}{E\,d\varepsilon}\right]^{-1} \frac{d\sigma}{d\varepsilon} = \frac{d\sigma}{d\varepsilon^p} \qquad (A1.4.1b')$$

A2 Experimental Principles

A2.1 Simple Tensile Test

In the present studies, this test is called " a tensile test ". Generally, metallic material expands due to tensile loading. Normally, a simple tensile test is performed to find material behavior under the uniaxial stress field without temperature variation. Inelastic strain rate goes up on the way of loading as shown in Figure A2.1.1. A simple tensile test is the same as the first quarter cycle of a cyclic or a fatigue test.

The phenomenon is characterized by hardening and strain rate dependency, while there are two kinds of hardening, the kinematic and the isotropic. It is very important how great the sensitivity of stress σ to strain rate $\dot{\varepsilon}$ is. If the scatter due to the test specimens is greater than the strain rate dependency, no discussion about the dependency may be possible.

A2.2 Cyclic Loading Test

In the present studies, this test is called " a cyclic test ". During a cyclic loading test, tensile and compressive loadings are given to a test specimen continuously and mutually.

Especially on low cycle tests, we can follow each hysteresis loop for each cycle on an analogue

recorder. Therefore, while the lifetime for the complete failure of material is normally focused at with high cycle loading, cyclic loading tests terminated before destroying test specimens may have some significance to check the hysteresis behavior. This is called a cyclic test, which differs from a fatigue test. In general, however, in both cases of cyclic loading tests and fatigue tests, the strain (sometimes stress or deformation) amplitude and the range should be decided. For example, with strain controlling operation, the strain amplitude and the range are selected as shown in Figure 4.3.2.1. Yield stress R becomes to be saturated following the cyclic number.

In the present studies, strain rate and strain range were shifted at random during experiments. In this case, isotropic hardening R should also be saturated at last. The sum of the stress histories for each constant strain range and strain rate can be regarded as the total history for the strain range and strain rate. On a cyclic test, the stress value increased continuously with increase in cycle number, which suggests that the isotropic hardening value has not yet been saturated. Over twenty cycles, the isotropic hardening reaches nearly the saturation value. Normally, it is not necessary to carry out a cyclic test to its saturation, where R_s means the stress value at the end of the cycles. On cyclic test V10, for example, no great shifting of stress value can be found out finally around the sixtieth cycle, which suggests that isotropic hardening can be regarded as being saturated.

A2.3 Creep test

Metallic material generally shows such behavior that strain on the material is initiated and propagated due to the holding stress which is less than the yield stress σ_y. This strain is a kind of inelastic strain, which is called creep strain. During a creep test, stress is kept at a certain positive or negative constant value for sufficiently long time.

Normally, the result is as shown in Figure A2.3.1. Creep can be divided into three domains in time history. In the first creep domain, creep strain rate, which starts from very high value, decreases with the increase in creep strain. During the secondary creep domain, creep strain rate is nearly constant independent of creep strain. In the final domain, the rate goes up again by creep strain. Strain rates during these primary, secondary and tertiary domains are shown in Figure A2.3.2. Here, the end of the secondary creep is approximately 80 or 90% of the lifetime during the creep test.

A creep test is reliable to see the material behavior related mainly with parameters K and n. It is, however, very difficult for some test machines to give a test specimen a constant stress condition from the beginning of a creep test. For example, a servohydraulic tension machine used in the present studies can not give the constant stress condition (see Figure A2.3.3) but the other stress history (see Figure A2.3.4). Hence, no result of the primary creep test is completely reliable to determine parameter values K and n, in general.

The obtained experimental results under hold stress value of σ_H = 250 MPa are taken into

consideration as an example, here. The primary creep appeared for 5 to 10 minutes from the beginning, then strain rate became nearly constant during the secondary creep. The initial value of the secondary creep strain was observed to be around 10%. During the secondary creep domain, back stress and isotropic hardening are close to but less than those saturated values.

A3 Basic Knowledge for a Neural Network

A3.1 Primitive Idea

The current computers have been developed for the purpose of repeated calculations which are humanly impossible. Their mission is essentially to carry out calculations exactly and faithfully along a given program. It is impossible for computers to carry out such vague and adaptable works, for examples, learning, analogizing, intuiting and recognizing, that human beings usually do. Table A3.1.1 compares the characteristics of current computers and human brains.

On the other hand, new types of computers have recently started to be developed and been applied to the execution of the above mentioned human works. These new types of computers have an internal system which is developed based on the structures and the functions of the human neuron. It is called " a Neural Network " or " a Neural Computer " in contrast to the current computers. The mission of the neural network is to anticipate vague and adaptable works which human brains usually do.

The position of the neural network in all the presently available computers is shown in Figure A3.1.1. The basic idea of the neural network is to predict a relationship based on pattern recognition without theoretical consideration. While some learning patterns are needed for prediction, no special theory or rule is necessary. Tables A3.1.2 and A3.1.3 indicate the characteristics of the neural network compared with the current computers and the fuzzy computers.

A3.2 Historical Background

The history of the neural network is rather long, and it has already been proposed in 1940's. The studies on the neural network then was, however, not sufficient. The pattern perception computer system " a Perceptron ", which were proposed by Rosenblatt in 1958 and was regarded as the best neural network at that time, was revealed its faculty limit by Minsky and Papert later. The studies on the neural network became decelerated after the event.

Recently, " Traveling salesman problem ", which was one of the problems without a proper method of solution, was settled using the neural network by Hopfield and Tank in 1985. This event gave a stepping stone to the beginning of the second period of neural network studies. The new learning algorithm " Back propagation " was developed by Rumelhart in 1986, which suggested the possibilities of development and usefulness of the neural network. Back propagation is called " Generalized delta rule " compared with the learning method of perceptron " Delta rule ". Table A3.2.1 shows the outline of the historical studies on the neural network.

Presently, the intensity of studies on the neural network is increasing, though it may be regarded as the first step, and further studies in both the basic and the application should be promoted. On the other hand, the development of a hard machine for neural network operation is going on.

A3.3 Primitive Performance

As mentioned above, the neural network predicts essentially a certain relationship. That is to say, the neural network predicts the corresponding results as output data from some informations given as input data. Here, input and output data should be presented numerically, while such a numerical presentation and any corresponding object can be related uniquely under one-to-one correspondence. For example, numerical presentations of stress values σ_1, σ_2, σ_3, ... related to strain values ε_1, ε_2, ε_3, ... are employed as input data for the configuration of a hysteresis curve as shown in Figure A3.3.1. In this presentation scheme, strain values ε_1, ε_2, ε_3, ... are fixed. Variation in the configuration of the hysteresis curves is expressed in terms of the variation of stress values σ_1, σ_2, σ_3, ...

The structure of the neural network is basically the same as that of the synapse on human nerve connections. Figure A3.3.2 shows the structure and reflection path of a unit. Every unit in the neural network corresponding to a human neuron is connected to one another with a weight corresponding to a synapse. On the real nerve system, a neuron reflects to an input signal which is informed through synapses and gives the answer signal corresponding to the importance (how much influence) and the direction (positive or negative influence) of its reflection. On the neural network, an output value is determined from the sum of the weighted input values at any unit. The

output data may become the input data for the other units or may directly be the final output of the whole network.

The connection systems of neurons on the surface and inside of the brain are different. On the brain surface, the narrow neurons which are 1 mm long are forming a line, where every signal is conveyed from the outside to the inside. The layer type neural network shown in Figure A3.3.3 is based on the surface neuron system, and data are conveyed from the input layer to the output layer. On the other hand, neurons inside the brain have complicated connections to one another, where any signal may be conveyed from any neuron to neuron. The random connecting type neural network as shown in Figure A3.3.4 is based on the inside neuron system, and data are conveyed from any unit to unit.

A3.4 Application Fields

As the neural network is applied to a certain relationship, the discussion of the primary necessity is to determine what to give the neural network as input data and what to obtain from it as output data. It is not always clear if the neural network can predict the relationship suitably, but it depends upon whether proper inputs with sufficient amount of data and outputs are chosen.

Such works, as information treating, simulation of the human social system, games and predictions, that humans do usually are considered as candidates for the applicable fields of neural networks. Table A3.4.1 shows some important fields such as character recognition, plant operation and structure identification where the neural network is used at present.

Examples of references =

Hajime NAKANO and et.al. : "Neuro Computer for beginners" Gijutsu-Hyoron sha, (1988).
Hajime NAKANO (Edited) : "Basic of Neuro Computer" Korona sha, (1990).

Table A3.1.1 : Characteristics of the current computers and human brain

	Computer	Brain
Valid works	Calculation	Pattern recognization, Total judgment
Technique	Secuential processiog	Parallel processing

Table A3.1.2 : Comparison of the characteristics of neural computer and current computer

Neural computer	Current computer
Pattern consideration (intuitional)	Logical consideration
Analogy reflection (moderate)	Digital reflection
Learning base (non-fixed, flexible)	Program

Table A3.1.3 : Comparison of the characteristics of neural computer and fuzzy computer

	Neural computer	Fuzzy computer
Developing way	Sample collection, learning	Rules, membership functions
Operation way	automatic	manual
Advantages	experience is not necessary	data is not necessary
Disadvantages	Exactitudei depend on learning data	Knowledge is difficult to collect
Inside Logic	unknown	Rules

Table A3.2.1 : Outline history of neural computer

1943 : Digital neural model with an on-off activation function (Mc Culloch and Pitts)
1949 : Hypothesis of learning of human brain (Hebb)
1958 : Perceptron (Rosenblatt)
1960 : Delta rule (Widrow and Hoff)
----- The first period of neural computer -----
1969 : Faculty limit of perceptron (Minsky and Papert)
----- Black period -----
1982 : Spinglass model (Hopfield)
1983 : Boltzmann machine (Hinton)
1986 : Back propagation and generralized delta rule (Pumelhart)
----- The second period of neural computer -----

Table A3.4.1 : Application fields of neural network.

Neural network : predicts the mother group from a sample group (interpolates)

Robot operation	Action operation (when to do, what to do) Practical operation (How to do)
Pattern recognization	Characters reading, Picture treating, Voice treating
Plant operation	Trouble searching during cooling procedure of melded steel

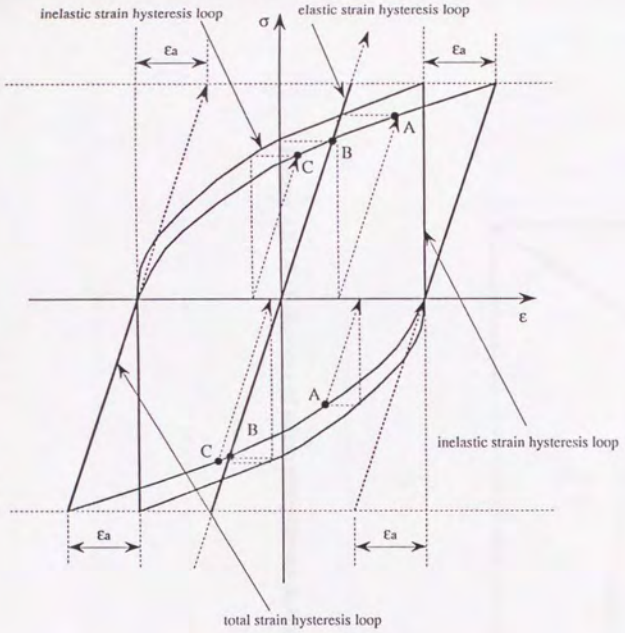

Figure A1.4.1 : Hysteresis loops corresponding to strain components during a cyclic test

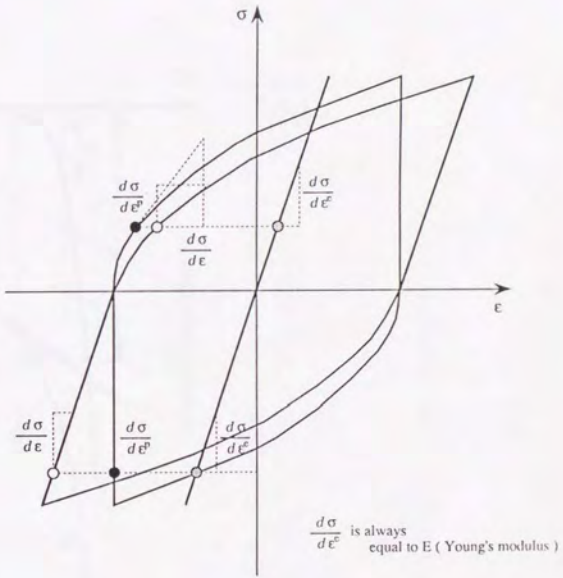

Figure A1.4.2 : Time-differential values of strain components

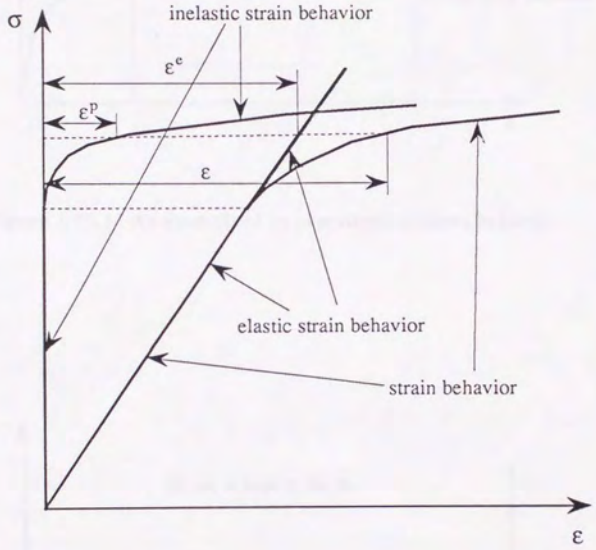

Figure A2.1.1 : Behaviors of strain components during a tensile test

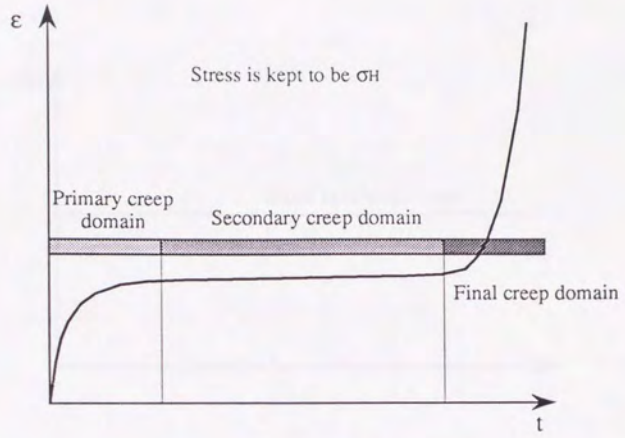

Figure A2.3.1 : An example of an experimental creep behavior

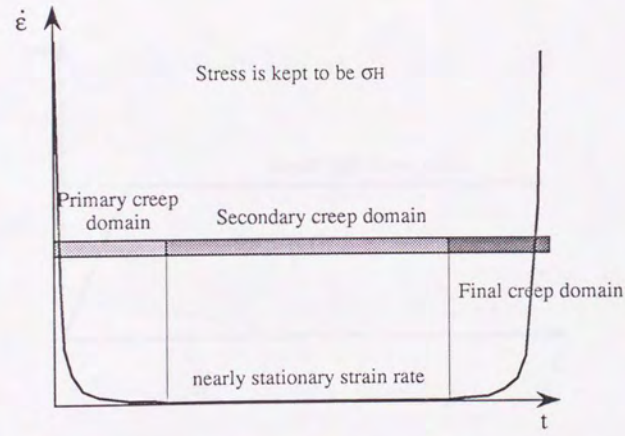

Figure A2.3.2 : An example of a strain rate behavior during a creep test

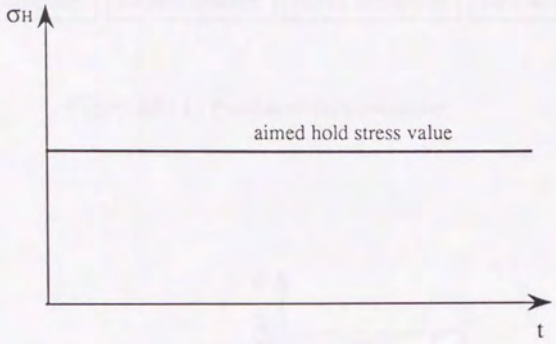

Figure A2.3.3 : An expected loading for a creep test

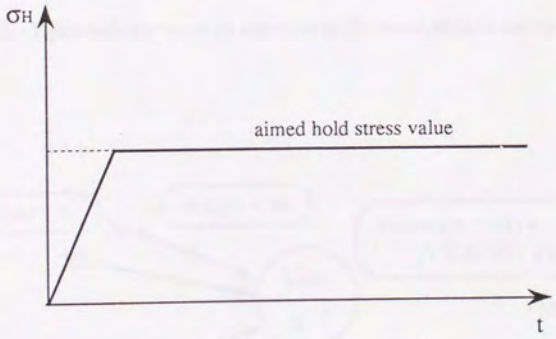

Figure A2.3.4 : An obtained loading for a creep test
(in the case of the employed test machine)

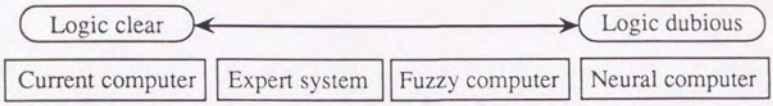

Figure A3.1.1 : Position of each computer

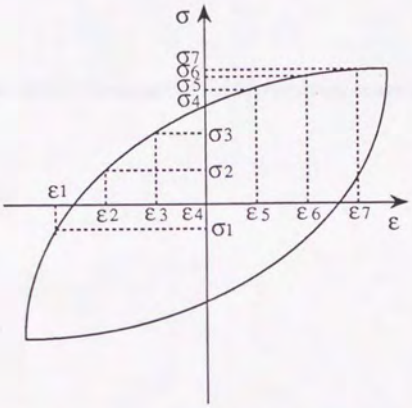

Figure A3.3.1 : Hysteresis curve as an example of the input data to the neural network

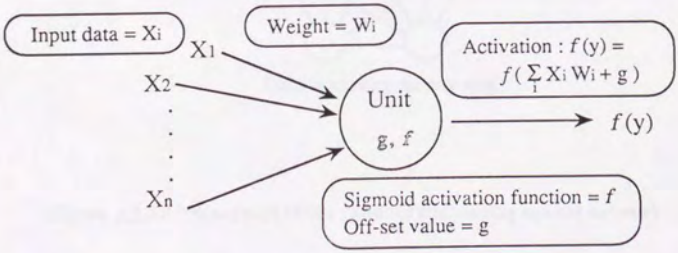

Figure A3.3.2 : Reflection of a neural unit

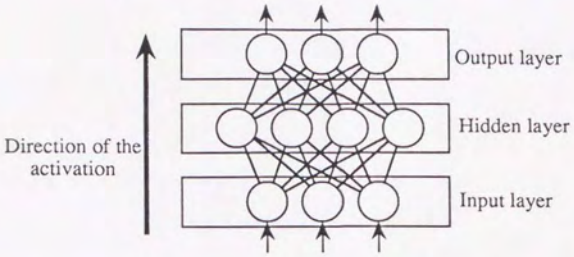

Figure A3.3.3 : Structure of the hierarchical neural network.

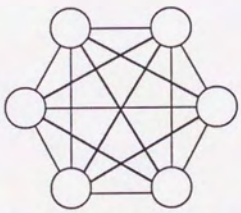

Figure A3.3.4 : Structure of the random connecting neural network

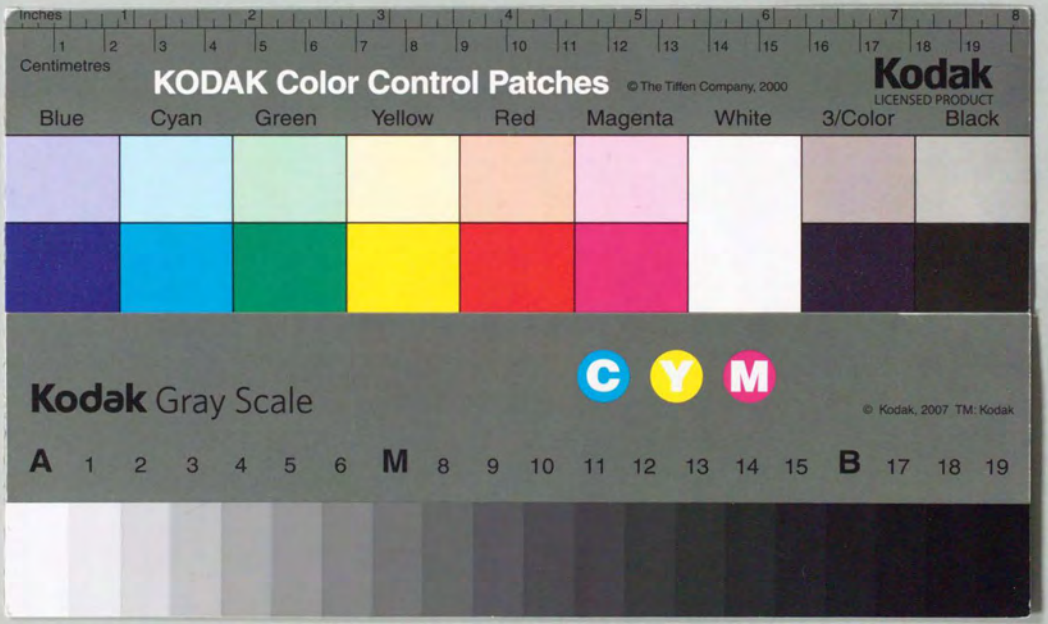
Inches
Centimetres
KODAK Color Control Patches
© The Tiffen Company, 2000
Kodak
LICENSED PRODUCT
Blue
Cyan
Green
Yellow
Red
Magenta
White
3/Color
Black
Kodak Gray Scale
C
Y
M
© Kodak, 2007 TM: Kodak
A 1 2 3 4 5 6 M 8 9 10 11 12 13 14 15 B 17 18 19